





Can Pseudotachylytes Form via Fracture-Induced Decompression Melting Under Hydrous Conditions?

Mattia Pistone ^{*1}, Virginia G. Toy ^{2,3}, Michael W. Ofman³, Eric Formo ⁴, Martin Robyr ⁵

¹Department of Geology, University of Georgia, Franklin College of Arts and Sciences, Geography-Geology Building, 210 Field Street, Athens, GA 30602-2501, United States of America | ²Institut für Geowissenschaften, Johannes Gutenberg-Universität Mainz, J.-J.-Becher-Weg 21, D-55128, Mainz, Germany | ³Department of Geology – Te Tari Tatai Arowhenua, University of Otago – Ōtākou Whakaihu Waka, 360 Leith Street, 9016, Dunedin, New Zealand | ⁴Georgia Electron Microscopy, University of Georgia, Interdisciplinary STEM Research Building 1, 302 East Campus Drive, Athens, GA 30602-2501, United States of America | ⁵Institute of Earth Sciences, University of Lausanne, Bâtiment Géopolis, Quartier UNIL-Mouline, CH-1015, Lausanne, Canton of Vaud, Switzerland

Abstract Frictional rock sliding and resultant shear heating along a fault plane are proposed as the necessary conditions to generate earthquake-related pseudotachylytes. However, frictional melting alone is energy expensive, requiring large temperature increases of several hundreds to thousands of degrees. Using the example of the pseudotachylyte structures of the Balmuccia Peridotite Massif (Ivrea-Verbano Zone, Alps, Italy), a minimum temperature increase of up to ~540°C for frictional melting has been proposed under isobaric and anhydrous conditions. Such conditions are however inconsistent with the moderate temperature increases, of up to ~400°C, and diminishing pressures, less than 0.7 GPa, required to form the observed A-type pseudotachylyte structures, with ultramafic composition corresponding to the melting of specific mineral phases as a function of Carboniferous Period pressure and temperature conditions. Here we show that pseudotachylytes could be produced by fracture-induced decompression melting under hydrous conditions, that favor the formation of immiscible liquids derived from melting Al-Cr spinel and orthopyroxene with suspended clinopyroxene minerals in this immiscible melt. We propose thermodynamic calculations that constrain phase stability in the pressure-temperature space of the Balmuccia lherzolite under both anhydrous and hydrous conditions (0.5 to 1 wt.% H₂O). We illustrate that the Al-Cr spinel+orthopyroxene composition of the pseudotachylyte is consistent with lower pressure conditions than those of the initial peridotite prior to fracturing. These thermodynamic calculations help determine the pressure-temperature path of pseudotachylyte formation, not only favored by frictional heating but also by pressure drop (0.3–0.9 GPa) following dilation related to rock fracturing. Our results call for a reassessment of the origin of many pseudotachylytes formed in the lower crust and upper mantle. We show that fracture-induced decompression melting under hydrous conditions can be a viable mechanism that assists frictional melting by reducing the temperature rise from ambient temperature to melting temperature by 18% to 74%. A similar process may be significant in producing other pseudotachylytes during tectonic movement of lithospheric blocks in the deep crust and upper mantle.

Executive Editor:
Janine Kavanagh
Associate Editor:
Dripta Dutta
Technical Editor:
Mohamed Gouiza

Reviewers:
Elisabetta Mariani
Anonymous 1
Anonymous 2

Submitted:
9 August 2023
Accepted:
23 July 2025
Published:
28 August 2025

1 Introduction

Pseudotachylytes are fossil remnants of ancient earthquakes generated along fault planes in lithospheric rocks during tectonic processes (Sibson, 1975; Austrheim and Andersen, 2004; Andersen and Austrheim, 2006; Lin, 2007; Di Toro et al., 2009). Pseudotachylytes help decipher the mechanisms of coseismic fault lubrication and slip-weakening (Spray, 1995; Magloughlin and Spray, 1992; Kanamori et al., 1998; Bouchon and Ihmlé, 1999; Hirose and Shimamoto, 2005; Di Toro et al., 2006a, 2011; Yao et al., 2023) associated with the propagation of seismic ruptures in the lithosphere. There is a general

consensus that pseudotachylytes are formed when frictional heat, abrasion, and comminution (Tsutsumi and Shimamoto, 1997a; Menegon et al., 2017, 2021; Spang et al., 2024; Aldrighetti et al., 2025) induce melting of the rock during rapid/fast seismic fault slip; slower slip does not produce sufficient heat concentrations to generate a melt (McKenzie and Brune, 1972; Lin and Shimamoto, 1998; Nielsen et al., 2008; Del Gaudio et al., 2009; Moris-Muttoni et al., 2022). Therefore, pseudotachylytes are solidified earthquake-derived frictional melts (Michalchuk et al., 2023). The melt also rapidly solidifies/quenches, typically to glassy material, i.e., pseudotachylyte (Wenk, 1978; Sibson, 1980; Spray, 1992; Trouw et al., 2010; Ferrand et al., 2018; Dai

*✉ Mattia.Pistone@uga.edu

et al., 2022), which is thus considered to be a robust benchmark of past seismic slip events (paleoseismicity; *Sibson* 1975). Relatively unaltered pseudotachylyte veins found in exhumed lithospheric massifs testify to the occurrence of seismic ruptures even in deep portions of the lithosphere where rocks tend to have a dominantly viscous response to tectonic stresses (*Obata and Karato*, 1995; *Dunkel et al.*, 2021).

Yet questions remain about how pseudotachylytes are generated in the deep lithosphere, where high differential stresses (>0.4 GPa; *Obata and Karato* 1995; >1 to 6 GPa; *Scambelluri et al.* 2017; *Campbell et al.* 2020; *Pennacchioni et al.* 2024; *Menegon et al.* 2021; *Toffol et al.* 2024) are required for faulting. Laboratory experiments simulating dynamic fault strength and frictional melting processes under ambient conditions (*Spray*, 1987, 1992, 1995; *Shimamoto and Tsutsumi*, 1994; *Tsutsumi and Shimamoto*, 1997a,b; *Hirose and Shimamoto*, 2005; *Hirose*, 2005; *Di Toro et al.*, 2006a,b; *Del Gaudio et al.*, 2009) have highlighted that coseismic slip velocities of ~1 m/s and large displacements of tens of meters produce microstructures similar to those found in natural pseudotachylytes hosted in mantle rocks (*Lin and Shimamoto*, 1998). In these tests, rock weakening is first associated with breaking of grain asperities and pulverization forming gouge material. Then, rapid (flash) temperature increase leads the rock to partially melt above the solidus temperature or completely melt above the liquidus temperature depending on the maximum temperature achieved: 1200°C to over 1650°C in peridotites (*Andersen and Austrheim*, 2006) and up to 1392 to 1850°C inferred from the melting point of end-member mineral phases (olivine, pyroxenes, and spinel) in the peridotite (*Del Gaudio et al.*, 2009). In this case, thermal runaway of several hundreds to thousands of degrees in quasi-steady-state, infinite-like ductile localization that weakens rocks by producing a molten shear band that lubricates the fault and sustains rupture propagation (*Ogawa*, 1987; *Karato et al.*, 2001; *Braeck et al.*, 2009; *Spang et al.*, 2024) may be a driver of earthquakes at great depth (*Green and Houston*, 1995; *Zhan*, 2020). The frictional melt rapidly flows and continuously coats the slip surfaces while the fault slips at velocities of 2 to 10 m/s (*Lin and Shimamoto*, 1998; *Ferrand et al.*, 2018). Following the host rock stress relaxation producing heat (*Spang et al.*, 2024), frictional or flash melting thus results in lubrication of the slip surface and weakening. But both suction into open fractures, and solidification of melt when shear heating reduces with heat loss due to cooling on lubricated surfaces (*Bjornerud and Magloughlin*, 2004), can lead to rock strength recovery and sliding arrest (*Ferrand et al.*, 2018). Recent experiments using cubic-anvil apparatus have simulated triaxial deformation of synthetic serpentinized peridotite at 1.1 GPa and have shown that rapid (0.1 to 10 seconds) and large temperature rises (>1250°C) can occur even with extremely small seismic slip on the order of 10 microns on tiny microfaults to generate pseudotachylytes (*Ferrand et al.*, 2017).

To date, experiments have supported the assumption that pseudotachylytes can form from the frictional melting of all the mineral phases along the fault plane in deep-seated (>40 km) deformational instabilities in relatively low-temperature environments (e.g., 700 to 900°C in mantle peridotites; *Kelemen and Hirth* 2007; *Ueda et al.* 2008, 2020; *Souquière and Fabbri* 2010). However, this mechanism is inconsistent with the actual geochemical composition of natural pseudotachylytes produced by melting selected mineral phases (starting from the minerals of low melting point; *Shand* 1916; *Spray* 1992) as a function of pressure (P), temperature (T), and under hydrous conditions. Specifically, the large temperature increases at isobaric conditions assumed for frictional melting do not explain the resulting pseudotachylyte composition produced at moderate temperatures (~1300–1450°C) and lower pressures (<0.7 GPa). We have inspected representative glassy pseudotachylytes in peridotites, by coupling a combination of micro- to nanostructural and geochemical analyses with thermodynamic modelling, to test the feasibility of rapid decompression melting under hydrous conditions. Decompression melting refers to a process in which a rock body, held at approximately the same temperature, experiences reduction in confining pressure (adiabat) until it achieves its solidus temperature above which the rock partially melts (*McKenzie and Bickle*, 1988). In this study, we consider fracture-induced decompression melting as a rapid geological process stimulated by a sudden pressure drop due to dilation, resulting from accommodating shear of rough surfaces or gouge without microscale fragmentation in Mode II/III fractures formed when Coulomb's criterion is met, and accommodating slip parallel to the crack surface (*Jaeger and Cook*, 1979; *Samuelson et al.*, 2009; *Brantut*, 2019). This fracturing mode might result in internal P reduction that leads the rock system (and the minerals therein) to surpass their solidus. In these types of fractures leading to the formation of pseudotachylytes, decompression would aid efficient generation of melts so less heat has to be produced by frictional work. However, whether partial melting due to decompression occurs or not depends on the petrology of the rock system and, thus, on two factors: where the rock system is originally positioned in P - T space, and the phase diagram topology, including the position of the rock solidus temperature modulated by the available water concentrated in hydrous minerals, nominally anhydrous minerals, and/or fluids along grain boundary regions within the rock (*Stünitz et al.*, 2024). Here we show that pseudotachylytes in peridotitic rocks in the lower crustal/upper mantle domain can be produced by partial melting instead of total melting of the original rock system along the fault plane. We propose that decompression-driven partial melting can be a crucial complementary mechanism assisting frictional melting during the generation of pseudotachylytes.

2 Geological Setting and History

2.1 The Balmuccia Peridotite Massif in the Ivrea-Verbanò Zone

A well-studied geological site where well preserved pseudotachylytes from the deep crust are exposed is the Balmuccia Peridotite Massif in the Ivrea-Verbanò Zone (Southern Domain of the Western Alps, Italy) (Obata and Karato, 1995; Ueda et al., 2008, 2020; Souquière and Fabbri, 2010; Souquière et al., 2011; Menegoni et al., 2024) (Figure 1). The Balmuccia Massif is one of the largest peridotite slivers in the Ivrea-Verbanò Zone and is one of the best exposed peridotites in the world. It is an elongated NNE-SSW trending lens of 4.5 km in length, 0.5 km in width, and 1.1 km in height (Shervais, 1979) that stretches from the surface down to 3-km depth with a downward broadening shape, that steeply inclines at $\sim 60^\circ$ towards the west with a gently inclined boundary of 30° to 40° towards the east (Ryberg et al., 2023). The Balmuccia peridotite is considered detached from the original Adriatic or Adria mantle (Quick et al., 1995) because it is bounded by extensional high-temperature shear zones (Brodie and Rutter, 1987; Brodie et al., 1992; Rutter et al., 1993) while being encapsulated in the deep lower crust made of Paleozoic granulite-facies metasedimentary units (Kinzigite and Stronalite Formations; Schmid and Wood 1976; Schnetger 1994; Redler et al. 2012) and the Lower Permian Mafic Complex (Basischer Hauptzug or Mafic Formation) of the Ivrea-Verbanò Zone (Zingg, 1983; Shervais and Mukasa, 1991; Quick et al., 1995, 2002; Handy et al., 2005; Rutter et al., 2007; Souquière and Fabbri, 2010) (Figure 1). Specifically, the Balmuccia Peridotite Massif is bounded to the west by a shear zone affecting the units of the Mafic Complex and Kinzigite Formation, and to the east by a <100-m wide zone of the “contact series” consisting of pyroxenites and meta-gabbro-norites (Shervais and Mukasa, 1991). The Balmuccia peridotite is the least depleted (or most fertile) and least metasomatized ultramafic body (Voshage et al., 1990; Sossi et al., 2018) along with the Baldissero and Premosello bodies in the exposed continental crustal section of the Ivrea-Verbanò Zone (Capedri et al., 1977; Ernst, 1978, 1981; Rivalenti and Mazzucchelli, 2000). The Balmuccia Massif comprises spinel lherzolite, which is the main lithology that dominates 85% of the ultramafic body (Rivalenti et al., 1975; Shervais, 1979), and minor spinel harzburgite and dunite, accompanied by pyroxenitic bodies (emplaced at 433 ± 75 Ma; Mazzucchelli et al. 2009) including websterites that are Cr-diopside-bearing and Al-augite-rich (Lensch, 1971; Shervais, 1979; Sinigoi et al., 1983) (Figure 2).

2.2 Structural Components of the Lherzolite

The foliations of the lherzolite strikes N-NE in the southern sector of the massif, approximately 005° , but strikes N-NW, approximately 350° , in the northern sector (Figure 1; Boudier et al. 1984). Dips range from 75 – 85° W in the southern sector to 45 – 75° W in the

northern sector. Some authors suggest that the original orientation of the foliation was close to horizontal, based on the hypothesis that the entire crustal section of the Ivrea-Verbanò Zone was uplifted and tilted through rotation along a N-S trending horizontal axis (Rivalenti et al., 1975; Zingg and Hunziker, 1990; Handy et al., 1999). A lineation defined through the orientation of accessory spinel grains in the plane of the foliation mainly plunges 45° to 65° towards 005° in the southern sector of the massif and mainly plunges 10° to 15° towards 350° in the northern sector (Figure 1; Shervais 1979; Boudier et al. 1984).

The lherzolite is commonly cut by planes of displacement, or macroscale “faults” mainly with <10 cm offset, which are associated with pseudotachylyte structures (Figure 2). The macroscale faults observed at the outcrop scale in the sampling location in this study (Figure 1) are perpendicular to the measured foliation strike and lineation trend (Boudier et al., 1984) as reported by Ferrand et al. (2018). Based on field observations, these macroscale faults appear to be oriented NE-SW with less common W-E and NW-SE strikes with dips of $>60^\circ$ (Figure 2) where field measurements were possible along planar face of the outcrop (see photo inset in Figure 1). NE-SW and NW-SE macroscale faults are observed to locally offset the clinopyroxene dikes by less than 4.5 cm. The offsets indicate both apparent sinistral and dextral shear sense (Figure 2).

The lherzolite displays a protoequigranular tabular texture associated to the strong foliation in the northeastern portion of the Balmuccia Massif while the southwestern sector of the Massif is characterized by a porphyroclastic texture of olivine and orthopyroxene (Garuti, 1977; Garuti and Friolo, 1979; Shervais, 1979; Boudier et al., 1984). In both rock textures, olivine always has a D-type fabric (Garuti, 1977). The lherzolite (60 to 70% olivine, 20 to 25% orthopyroxene, 12 to 13 vol.% clinopyroxene, <1 to 3 vol.% spinel, and <1 vol.% amphibole) as the main lithology of the Balmuccia Massif is composed of forsteritic olivine, diopsidic clinopyroxene (ranging from $\text{Wo}_{50}\text{En}_{50}\text{Fs}_0$ to $\text{Wo}_{50}\text{En}_{45}\text{Fs}_5$) in contact with enstatitic orthopyroxene ($\text{Wo}_{1}\text{En}_{88}\text{Fs}_{11}$), Fe^{2+} -bearing spinel and Al-spinel with up to 9 wt.% Cr_2O_3 (Al-Cr spinel) located at triple points as well as inclusions in olivine (Garuti and Friolo, 1979; Shervais, 1979; Sinigoi et al., 1983; Skrotzki et al., 1990, 1991).

2.3 Equilibration History of the Peridotite Massif

The original peridotite massif is thought to have equilibrated at $T = 1100$ – 1200°C and $P = 1.3$ – 2.0 GPa (Shervais, 1979) in the mantle during Variscan subduction processes (320–350 Ma) involving the subduction of the Rheic oceanic crust, the deposition of metasediments in an accretionary prism, and their burial, imbrication, and prograde metamorphism (Wyatt et al., 2022) to amphibolite and granulite facies (Schmid and Wood, 1976; Redler et al., 2012). During the

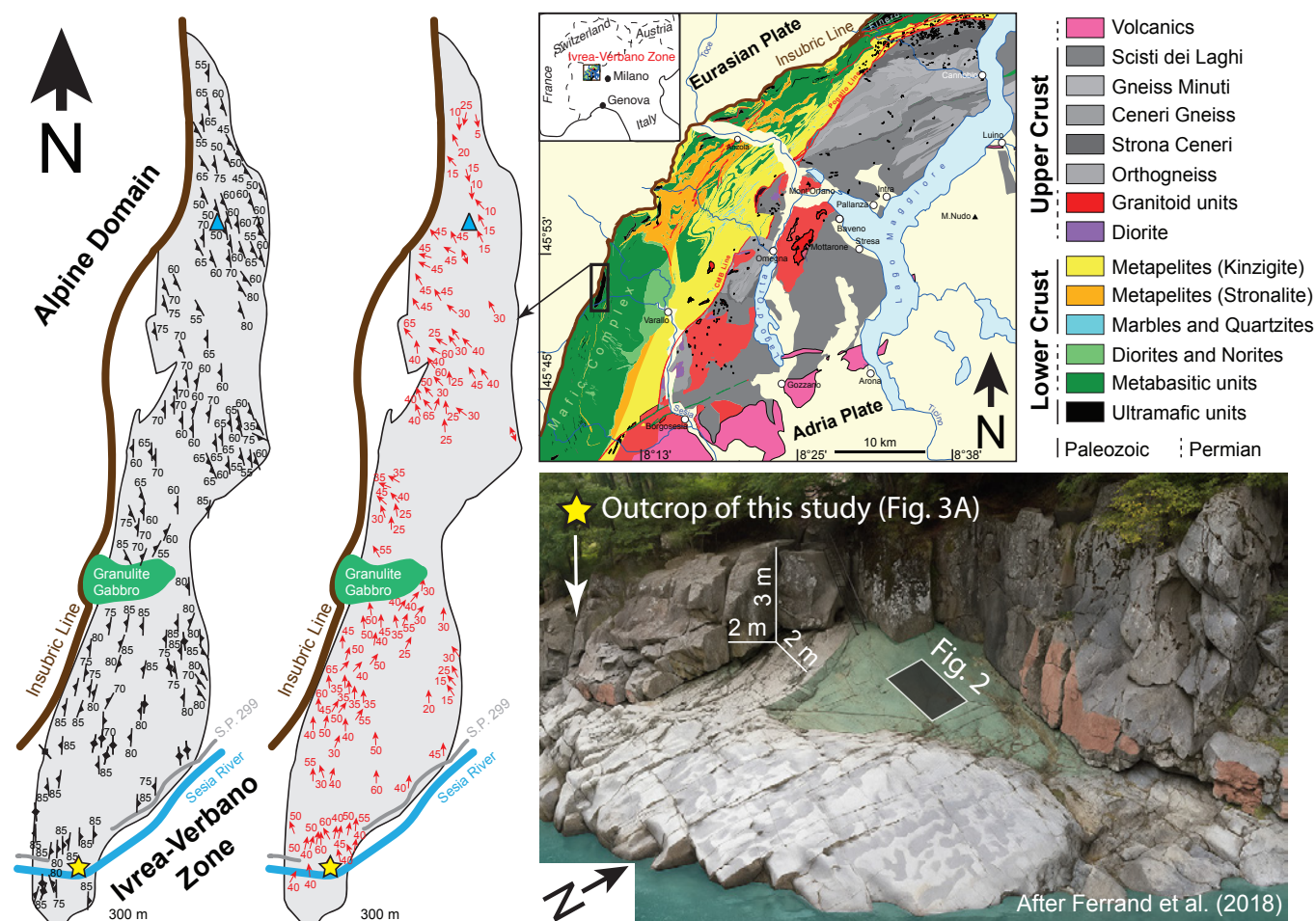


Figure 1 – Geologic context of the Ivrea-Verbano Zone and Balmuccia Peridotite Massif. Geological map of the Ivrea-Verbano Zone (Alps, Italy) (modified after *Brack et al.* 2010, based on the works of: *Rutter et al.* 1999; *James* 2001; *Schaltegger and Brack* 2007) with the Insubric Line (brown line) dividing the Adria plate (southeast) from the Eurasian plate (northwest) and major pre-Alpine fault zones (red lines). The inset image shows the location of the Ivrea-Verbano Zone in Italy (modified after *Rutter et al.*, 2003). The outline of the Balmuccia Peridotite Massif is shown, with measurements of foliation strike and dip (black symbols) and lineation trend and plunge (red arrows), measured principally through the orientation of spinel grains (*Shervais*, 1979; *Boudier et al.*, 1984). Note that many measurements of foliation also include deformed Cr-websterite dikes in the same orientation (*Boudier et al.*, 1984). We do not report the internal lithological subdivision (lherzolite, dunite, and pyroxenites) of the Balmuccia Peridotite Massif as shown in the work of *Shervais* (1979), structural data related to fault and dip, fold axis, dextral and sinistral minor fold axis as shown by *Shervais* (1979) and *Boudier et al.* (1984), and major discontinuities within the ultramafic body as revealed by the drone-based photogrammetry of *Menegoni et al.* (2024). The Insubric Line (thick brown line) includes the Tonnello Fault in proximity of the southern portion of the Balmuccia Peridotite Massif. The yellow star indicates the sampling location of the lherzolite outcrop characterized by the presence of pseudotachylite structure. The location of the outcrop of this study (Figure 3A; N 45°49'13.0", E 8°09'15.6", elevation of 553 m a.s.l.) is located in the upper portion of the rock outcrop investigated by *Ferrand et al.* (2018). The view of the outcrop from the right bank of the Sesia River is from *Ferrand et al.* (2018) devoid of the original sketches which were removed using the 3.5 model of the Generative Pre-trained Transformer (OpenAI Inc., USA). The green-shaded area of the outcrop is from *Ferrand et al.* (2018) indicating the eroded injection plane displaying the remnants on the bottom surface of the tensile fracture. In this outcrop portion, manual field drawing was applied using a tracing paper in which structural and lithological features were recorded at an accuracy down to the subcentimeter scale (see inset grey rectangle of 2.73 x 2.03 m, which is detailed in Figure 2). The outcrop face targeted in this study (indicated by the yellow star) is perpendicular to the polished outcrop surface and has a W-E trend. The light blue triangle indicates the Cima di Lavaggio, the summit point of the Balmuccia Peridotite Massif. S.P. = Strada Provinciale.

late stage of the precursor Variscan orogeny, relatively homogenous mantle deformation occurred at the scales of a few kilometers to a few tens of kilometers (*Drury et al.*, 1991). During the Carboniferous Period (300–320 Ma), the Balmuccia peridotite was exhumed from the mantle and emplaced in granulite-facies metasedimentary units in the lower crust, within the Ivrea-Verbano Zone (*Lensch*, 1971; *Rivalenti et al.*, 1975; *Ernst*, 1978; *Shervais*, 1979; *Shervais and Mukasa*, 1991), probably

at $T = 720\text{--}900^{\circ}\text{C}$ and $P = 0.9\text{--}1.1\text{ GPa}$ (*Handy et al.*, 1999).

More specifically, the exhumation of the mantle peridotite likely occurred $\sim 316\text{--}275$ million years ago (*Peressini et al.*, 2007; *Klötzli et al.*, 2014) during the initial period of magmatic underplating (*Voshage et al.*, 1990) producing magmas derived from the hydrous mantle source (*Berno et al.*,

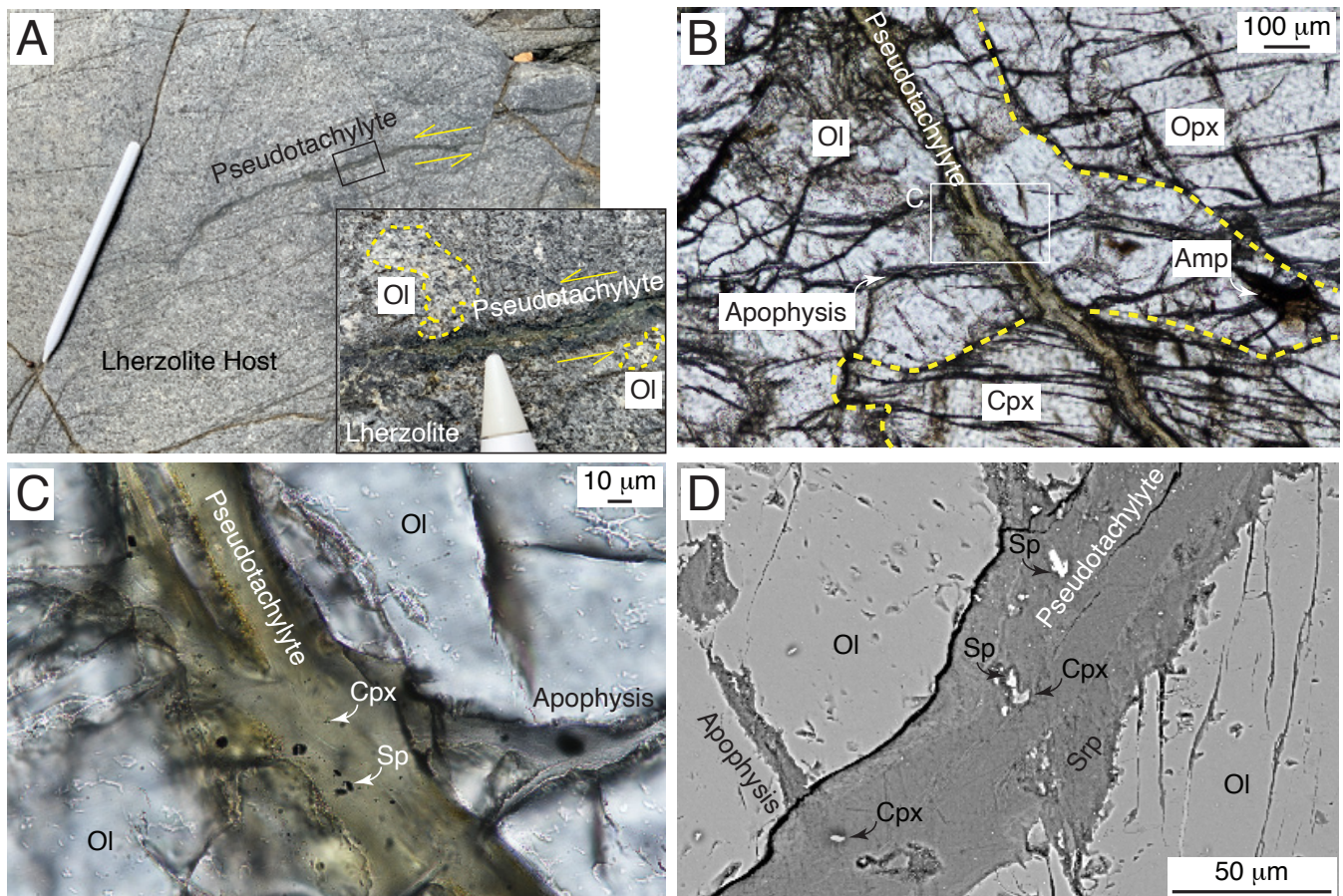


Figure 3 – A-type Pseudotachylite in Balmuccia lherzolite. **A)** Field view of the pseudotachylite in lherzolite host with central serpentinized portion (pencil length = 176 mm) showing 1-cm displacement of olivine minerals (highlighted by yellow dashed contours). **B-C)** Pseudotachylite viewed using the unpolarized light with optical microscope. **D)** SEM-based BSE image of pseudotachylite with dispersed clinopyroxene and rims of spinel and possible serpentine. Abbreviations: Amp = amphibole, Cpx = clinopyroxene, Ol = olivine, Opx = orthopyroxene, Sp = spinel, Srp = serpentine.

2020). During exhumation, deformation of the mantle rock was accommodated in anastomosing networks of centimeter- to hundred-meter-wide shear zones that may also serve as sites for late-stage fluid percolation (Drury *et al.*, 1991). The peridotite and adjacent metasedimentary granulite complex were then exhumed during the Permian transtension (270–290 Ma; Handy *et al.* 1999; Petri *et al.* 2019) and Triassic-Jurassic rifting of the Piemonte-Liguria Ocean (180–230 Ma; Handy and Stünitz 2002). During this period, the peridotite experienced a high-temperature ($\sim 1000^{\circ}\text{C}$) and low stress (~ 20 MPa) intrusion into the lower crust as manifested in the coarse-grained dynamically recrystallized olivine (Skrotzki *et al.*, 1990) and in the deformation microstructures in the shear zones bordering the pseudotachylites (Jin *et al.*, 1998). Then, during the Tertiary Alpine collision, the peridotite experienced brittle deformation along the Periadriatic Lineament or Insubric Line (the tectonic boundary separating the African promontory Adria from the Eurasian plate with a dextral sense of shear suggested by the tectonic line gently dipping to the north; Zingg and Hunziker 1990; Figure 1) and crustal overprinting during tilting of the crustal section of the Ivrea-Verbano Zone (Handy *et al.*, 1999; Rutter *et al.*, 2007).

The second deformation event evidently occurred at relatively low temperature ($\sim 650^{\circ}\text{C}$) and high regional or overburden stress (~ 300 MPa) (Skrotzki *et al.*, 1990). This deformation event is recorded in the fine-grained dynamically recrystallized rims around the matrix grains, in the subgrain size and dislocation density in olivine within the porphyroclastic domain, and in clinopyroxene lamellae in orthopyroxenes (Skrotzki *et al.*, 1990, 1991). The Cenozoic deformation preserved traces of the pre-Alpine fabrics and mineral assemblages in the Balmuccia lherzolite (Schmid *et al.*, 1989). During these tectonic processes ranging from the Variscan orogen collapse to the Alpine orogenesis, the peridotite sliver of the Balmuccia Massif experienced macroscale fault displacements with common production of pseudotachylites (Techmer *et al.*, 1992; Obata and Karato, 1995). Based on the combination of geochronology and field relations, two groups of pseudotachylite structures are found in the Balmuccia Massif: an A-type group (350–270 Ma; including Groups 1 and 2 pseudotachylites based on the classification of Ueda *et al.* 2020) largely attributed to the Carboniferous stages of the Variscan orogeny or during the subsequent Permian trans-tension at $550\text{--}900^{\circ}\text{C}$ and $0.6\text{--}1.2$ GPa, and a B-type group (<70 Ma; Group 3 of Ueda

et al. 2020) related to the Alpine orogeny at $<600^{\circ}\text{C}$ (Wiederkehr *et al.*, 2008, 2009) and $<0.3\text{ GPa}$ (Souquière and Fabbri, 2010; Souquière *et al.*, 2011; Ferré *et al.*, 2017). In this study, we focus on the A-type pseudotachylyte structures, which seem to represent the features that best record deep earthquake processes in the upper mantle/lower crustal domain. These pseudotachylytes characteristically crop out as $<1\text{-mm}$ to 2-cm thick structures having sharp boundaries with the host lherzolite (Figures 2 and 3A). Most of the A-type pseudotachylyte structures strike between 140° and 230° and dip more than 65° towards the east (Figure 2).

3 Methods

3.1 Fieldwork

Fieldwork was carried out to identify, characterize, and sample A-type pseudotachylytes at the outcrop scale in the Balmuccia Peridotite Massif. We collected field observations at the outcrops of lherzolites along the north bank of the Sesia river at N $45^{\circ}49'13.0''$ and E $8^{\circ}09'15.6''$ (as measured using a Garmin eTrek 10), about 60 m south of the Strada Provinciale 299, located halfway between the localities of Balmuccia (SSW) and Isola di Vocca (NNE). Rock sampling was conducted by selecting and chipping (with hammer and chisel) five pseudotachylytes (and the host rock around) displaying a thickness of $<5\text{ mm}$, devoid of alteration/devitrification, with clear evidence of mineral phase displacement (possibly as a result of one single event of displacement with no continuous reactivation of the same fracture zone), and devoid of apophyses at the scale of the rock outcrop. Such a selection helped mitigate a number of complexities for the forthcoming geochemical and micro- to nanostructural analyses and ensured the identification of the mineral phases and the petrological assessment of frictional melting versus decompression melting. In particular, the limited thickness of the pseudotachylyte on the millimeter scale represents an ideal case where near-equilibrium conditions can be achieved during rock friction, melting, and pseudotachylyte formation, with efficient heat transfer in a limited mass of material, mass conservation (without major apophyses), and identifiable unmelted and melted components in the pseudotachylyte and the surrounding fractured rock. Hence, near-equilibrium conditions are petrologically quantifiable using thermodynamic constraints. The selection of pseudotachylyte devoid of alteration/devitrification was based on the material color and smooth appearance. In particular, dark/black color of the whole pseudotachylyte or the outer rims of it are suggestive of ultramafic material possibly glassy without greenish or reddish coloration, which tends to be associated to geochemical modifications induced by serpentinization and/or oxidation occurring after the generation of the pseudotachylyte (Trouw *et al.*, 2010).

3.2 Analytical Investigations

Rock textural analysis was conducted using different techniques. The selection of the pseudotachylyte to inspect analytically was based on the glassy appearance of the material via optical microscopy. Optical observations of three (out of five) pseudotachylytes in thin section were acquired using a Nikon Eclipse LV100N POL petrographic microscope at the Department of Geology of the University of Georgia (USA). Microstructural analysis of the same rocks was conducted using backscattered electron (BSE) imaging at 15 kV accelerating voltage and 1 nA beam current on a Thermo Fisher Scientific Teneo field emission scanning electron microscope (SEM). We then focused on one single sample of pseudotachylyte showing the largest thickness of the inner unaltered glassy portion for geochemical characterization via secondary electron (SE) imaging using a Hitachi SU-9000 low voltage scanning transmission electron microscope (STEM) (San Gabriel *et al.*, 2024) at the Georgia Electron Microscopy Center of the University of Georgia. Major element analysis of the experimental glasses was performed on the same pseudotachylyte with a JEOL JXA-8350F HyperProbe (EPMA) at the Institute of Earth Sciences of the University of Lausanne (Switzerland), using a 5 nA beam current and $1\text{ }\mu\text{m}$ beam diameter for nominally anhydrous minerals (clinopyroxene, orthopyroxene, olivine, and oxides), and $10\text{ }\mu\text{m}$ beam diameter for amphibole and glassy pseudotachylyte. The counting times on the peak and background positions were 30 and 15 s for Al, Ti, Ca, Mg, and Mn and 10 and 5 s for Si, Fe, Na, K, P, and Cl, respectively. Natural and synthetic standards were used and data were ZAF-corrected (Armstrong, 1988), including secondary glass standards of hydrous (5.7 wt.% H_2O) basalt (Müntener *et al.*, 2001). X-ray distribution maps of Si, Al, and Mg were acquired using the Oxford large area windowless energy dispersive spectroscopy (EDS) of the STEM at 30 kV and $10\text{ }\mu\text{A}$. Retrieval of standard chemical formulas for minerals from chemical analyses is based on spreadsheet recalculations here reported: https://serc.carleton.edu/research_education/equilibria/mineralformulaerecalculation.html.

3.3 Calculations of Melt Polymerization

Using the pseudotachylyte glass composition measured via EPMA, we estimate the first-order approximation to the degree of polymerization of the original melts forming the pseudotachylytes using the numbers of non-bridging oxygens per tetrahedra described by the NBO/T parameter (Giordano *et al.*, 2008). The NBO/T parameter is calculated according to the formulation proposed by Mysen (1988) by assuming that SiO_2 , TiO_2 , Al_2O_3 , and Fe_2O_3 are network formers and total iron (FeO_T) is split equally between FeO and Fe_2O_3 (Giordano and Dingwell, 2003; Giordano *et al.*, 2006). Such a calculation is applied under anhydrous conditions. Under hydrous conditions, we are not able to assess the exact amount of H_2O dissolved in the glass based on the volatile by-difference method from EPMA analysis of pseudotachylyte composition (Fleet

and Pan, 1995) due to the unavoidable inclusion of the serpentinized olivine rims or devitrified borders of the pseudotachylyte during EPMA measurements which yield for water concentrations higher than those expected for the unserpentinized portion of the pseudotachylyte.

3.4 Mass Balance Calculations

The evaluation of the melted components (produced via melting of original mineral phases) contributing to the bulk composition of pseudotachylyte is conducted using a combination of chemical analyses of each mineral and glass phase (using EPMA analysis of mineral phases and STEM-based EDS analysis of glass phase), the volumetric fraction of each phase in the pseudotachylyte (through inspection using optical microscopy, SEM-based BSE imaging, and STEM-based SE imaging), and the set of mass balance calculations based on the algorithm of Albaredo and Provost (1977) and the linear algebra formulation described by Draper and Johnston (1992). The system of equations in the mass balance is represented by the matrix expression $Ax = B$, in which A is the matrix of phase compositions, x is the vector of the weight proportions of each phase, and B is the vector representing the bulk composition of the pseudotachylyte on the anhydrous basis. Mass balance calculations (including propagation of errors from microscale EPMA analysis and nanoscale EDS-based data) were set up to four coexisting phases (olivine, orthopyroxene, clinopyroxene, and Al-Cr spinel) to evaluate the minerals and their proportions contributing to the bulk composition of pseudotachylyte. This mass balance calculation is also accompanied by the isocon analysis (Grant, 1986, 2005) based on the Grensers' (Grensens, 1967) equation quantifying the composition–volume relations between measured pseudotachylyte (on the anhydrous basis) and pseudotachylyte obtained by melting olivine, orthopyroxene, clinopyroxene, and spinel in different modal proportions. This approach further helps evaluate the conservation of the chemical components during the melting process forming the pseudotachylyte and the efficiency of partial melting of minerals contributing to the composition of the pseudotachylyte.

3.5 Calculations of Diffusion of Heat, Water, and Chemical Elements

In the discussion section (section 5.2), we estimate the timescales of diffusion of heat, major elements, and H_2O to evaluate whether pseudotachylytes are formed under equilibrium or disequilibrium conditions. In the latter scenario, within the duration of formation of pseudotachylyte, we expect to observe evidences of incomplete melting, crystallization, inefficient heat transfer, and/or mass loss that underline potential disequilibrium conditions. Both heat and chemical diffusion are described by the first law of Fick (Fick, 1855) that relates the diffusive flux to concentration (of heat or a chemical component) in a spatial derivative under the assumption of steady state. Unidimensional (1D) heat or thermal diffusion timescale with a characteristic length scale (which is equivalent to the

thickness of the pseudotachylyte considered in this study) and thermal diffusivity are estimated using the Fourier number (*baron de Fourier*, 1822). Diffusion of chemical components in melt during the melting process is described by the second law of Fick (Fick, 1855) that predicts how diffusion causes the concentration to change with time. Water diffusion is described by the simple approximation of the H_2O diffusion length scale $l = \sqrt{t \times D_{H_2O}}$ (Watson, 1982; Baker, 1991) with t as timescale and D_{H_2O} as water diffusivity determined using the pressure-dependent formulation of Ni and Zhang (2008). The formation of equilibrium conditions of glassy pseudotachylyte occurs when the following conditions are met: i) the thermal diffusion timescale is shorter than the frictional melting duration (0.1 to 10 seconds; Ferrand et al. 2018), which allows the rapid and complete melting of the specific mineral phases during thermal runaway (Spang et al., 2024) at certain pressure and temperature conditions; and ii) the timescale of chemical diffusion of both major elements and water in the melt is longer than the duration of melting and cooling processes leading to pseudotachylyte formation, implying that crystallization and modification of the associated glass composition do not occur in the pseudotachylyte.

3.6 Thermodynamic Modelling

To the goal of offering a thermodynamically rigorous petrological assessment of pseudotachylyte formation in the discussion (sections 5.3-5.4), we used the software package Perple_X (Connolly, 1990, 2005) (version 6.8.1) to compute stable mineralogy and phase diagrams (i.e., pseudosections; Connolly and Pettrini 2002) as a function of P - T for the Balmuccia anhydrous and hydrous (0.5–1.0 wt.%) lherzolite composition (Hartmann and Hans Wedepohl, 1993) by Gibbs free energy minimization (Connolly, 2009). We used the thermodynamic database labelled as HP02, which includes the dataset of end-member properties of Holland and Powell (1996) and solid-solution models for olivine—O(HP), garnet—Gt(HP) (Holland and Powell, 1996), pyroxenes—Cpx(HP) and Opx(HP) (Holland and Powell, 1998), plagioclase—Pl(I1,HP) (Holland and Powell, 2003), spinel—Sp(HP) (Jamieson and Roeder, 1984), and amphibole—Amph(DHP) (Dale et al., 2000). We explore the different stability fields of melt-free and melt-bearing mineral assemblages divided by the respective anhydrous and hydrous solidus temperatures in a wide range of pressure (0.0001 to 4 GPa) and temperature (700 to 1600°C). The P - T space in these phase diagrams allows to summarize the P - T evolution of the Balmuccia lherzolite through time (from 433 to 180 Ma) in a large depth range from 124 km to surface using the hydrostatic/lithostatic pressure equation $P = P_0 + \rho gh$, where P_0 is the atmospheric pressure, ρ is the spinel lherzolite density of 3300 kg/m³, g is the average gravitational acceleration of 9.81 m/s², and h is depth. The spinel lherzolite density is derived from previous Perple_X calculations of Pistone et al. (2020) reporting estimates ranging from 3305 to 3325 kg/m³ in the pressure range of 0.9-1.6 GPa at <700°C.

In the chosen P – T space, we explore and compare the conditions of frictional melting and decompression melting forming A-type pseudotachylyte between 700°C, below which the lherzolite is a “frozen” lithology (Ewing *et al.*, 2015; Smye *et al.*, 2019) using an average continental geotherm from Christensen and Mooney (1995), and 1600°C chosen just above the reference peritectic reaction temperature of 1557°C at 0.0001 GPa of forsterite-enstatite in the forsterite-SiO₂ binary phase diagram (Bowen and Andersen, 1914; Creig, 1927). Within the proposed P – T space, we expect that the formation of A-type pseudotachylyte occurs between 0.9 and 1.1 GPa, which is the originally proposed pressure range of formation of A-type pseudotachylytes (Handy *et al.*, 1999; Ueda *et al.*, 2008), and lower pressure conditions at which decompression melting should assist frictional melting process.

4 Results

The microstructural analysis shows that a microscale pseudotachylyte cross-cuts the primary minerals (olivine and pyroxenes) of the lherzolite (Figure 3B–C), displacing them sinistrally with an offset of ~1 cm based on the displacement of light-colored olivine (see yellow dashed lines surrounding the olivines in Figure 3A). The central portion of the pseudotachylyte appears to be mainly glassy owing to its transparent to weakly absorbent aspect to transmitted light using the petrographic microscope (Figure 3C). Potentially serpentinized olivine rims or devitrified pseudotachylyte boundaries are found at the periphery of the pseudotachylyte in contact with the host rock and contain accessory spinel along the olivine-pseudotachylyte contacts (Figure 3D). Serpentine is related to late-stage fluid percolation accompanying deformation at lower temperatures (200–400°C) during Alpine orogenesis (Handy and Stünitz, 2002; Ueda *et al.*, 2020); thus, serpentine is not associated to the original A-type pseudotachylyte composition. Microscopic apophyses (50 to 200 μ m long) are found along the primary pseudotachylyte feature (Figure 3B–D) and are suggestive of limited mass transport (<5% of the pseudotachylyte vein area observed in thin section; Figure 3B) from the main pseudotachylyte vein. A few suspended grains of clinopyroxene are found in the central portion of the preserved glassy pseudotachylyte (Figure 3D) in agreement with previous observations of the same minerals in amorphous pockets within ultramylonite-like veins found in the Balmuccia peridotite (Ferrand *et al.*, 2018). Accessory amphibole located at the boundaries of primary minerals cross-cut by pseudotachylytes (Figure 3B) are associated to percolation of hydrous (H₂O-bearing) mafic melts in the peridotite from sublithospheric mantle metasomatized during subduction processes in the Variscan prior to the Carboniferous emplacement of the peridotite in the lower crust (Mazzucchelli *et al.*, 2009), thus also prior to the formation of A-type pseudotachylytes. Minerals in the lherzolite (forsteritic olivine, diopsidic clinopyroxene [Wo₄₉En₄₇Fs₄], enstatitic orthopyroxene [Wo₁En₉₀Fs₉], Al-Cr-spinel, and pargasitic amphibole) were identified

through quantitative analyses of major elements using EPMA (see supplementary data at Pistone, 2025). On the anhydrous basis, the chemical composition of the pseudotachylyte is mainly made by SiO₂ (48 wt.%) and MgO (44 wt.%) followed by FeO_T (6.5 wt.%), and a limited concentration of Al₂O₃ (1 wt.%), while the same composition is CaO-poor (0.1 wt.%) along with MnO (0.1 wt.%), TiO₂ and Na₂O (<< 0.1 wt.%), and has no K₂O (see supplementary data at Pistone, 2025). Nanoscale analysis of the glassy portion of the pseudotachylyte (devoid of the serpentinized olivine rims or devitrified pseudotachylyte borders reported in Figure 3D) reveals droplets of amorphous materials separated by curvilinear contacts (Figure 4) and the presence of distinctive nanometer clinopyroxene minerals displaying sharp corners or edges suspended in the glass matrix (Figures 3C–D and 4). Through the geochemical inspection, we identify that the matrix appears to be made of two glasses derived from melting Al-Cr spinel and orthopyroxene, respectively, as observed in the chemical profiles and maps of Si, Al, and Mg (Figure 4). These chemical analyses reveal that the glass composition is best described by a coordination of 12 oxygens per formula unit, which is inconsistent with the stoichiometric oxygen coordination expected for the cation occupancy in minerals such as spinel (4 oxygens per formula unit) and orthopyroxene (6 oxygens per formula unit). The excess number of oxygens is suggestive of presence of unmeasured volatile component. The presence of volatile components (e.g., H₂O) is also suggested by low EPMA totals (~85 wt.%) for pseudotachylyte compositions (see supplementary data at Pistone, 2025), although such as EPMA totals are acquired at microscale with defocused beam (10 μ m) used for amorphous phases and thus are partly affected by the presence of serpentinized olivine rims or devitrified pseudotachylyte material included in the analysis. Under anhydrous conditions, the two glasses are characterized by NBO/T values of: 2.36 for depolymerized orthopyroxene glass (due to large concentration of network modifiers such as MgO) and 0.17 for polymerized Al-Cr spinel glass (due to the presence of network formers such as Al₂O₃). Under hydrous conditions, the NBO/T parameter would increase with increasing NBO in presence of H₂O added into the melt (Mysen, 2014). The isocon analysis showcases that the slope of the isocon of all major elements with concentrations >1 wt.% is 1±0.1, except for Al₂O₃ and FeO_T having isocon slopes of 0.4±0.1 and 0.8±0.1, respectively. Both isocon slopes for Al₂O₃ and FeO_T are sensitive to the low spinel modal proportion (<1 vol.%), in the studied lherzolite.

5 Discussion

5.1 Nanoscale Analysis Reveals the Fusible Mineral Components Forming Pseudotachylytes

At nanoscale, we identify two melted components (Al-Cr spinel and orthopyroxene) forming the glass matrix of the pseudotachylyte and one unmelted component

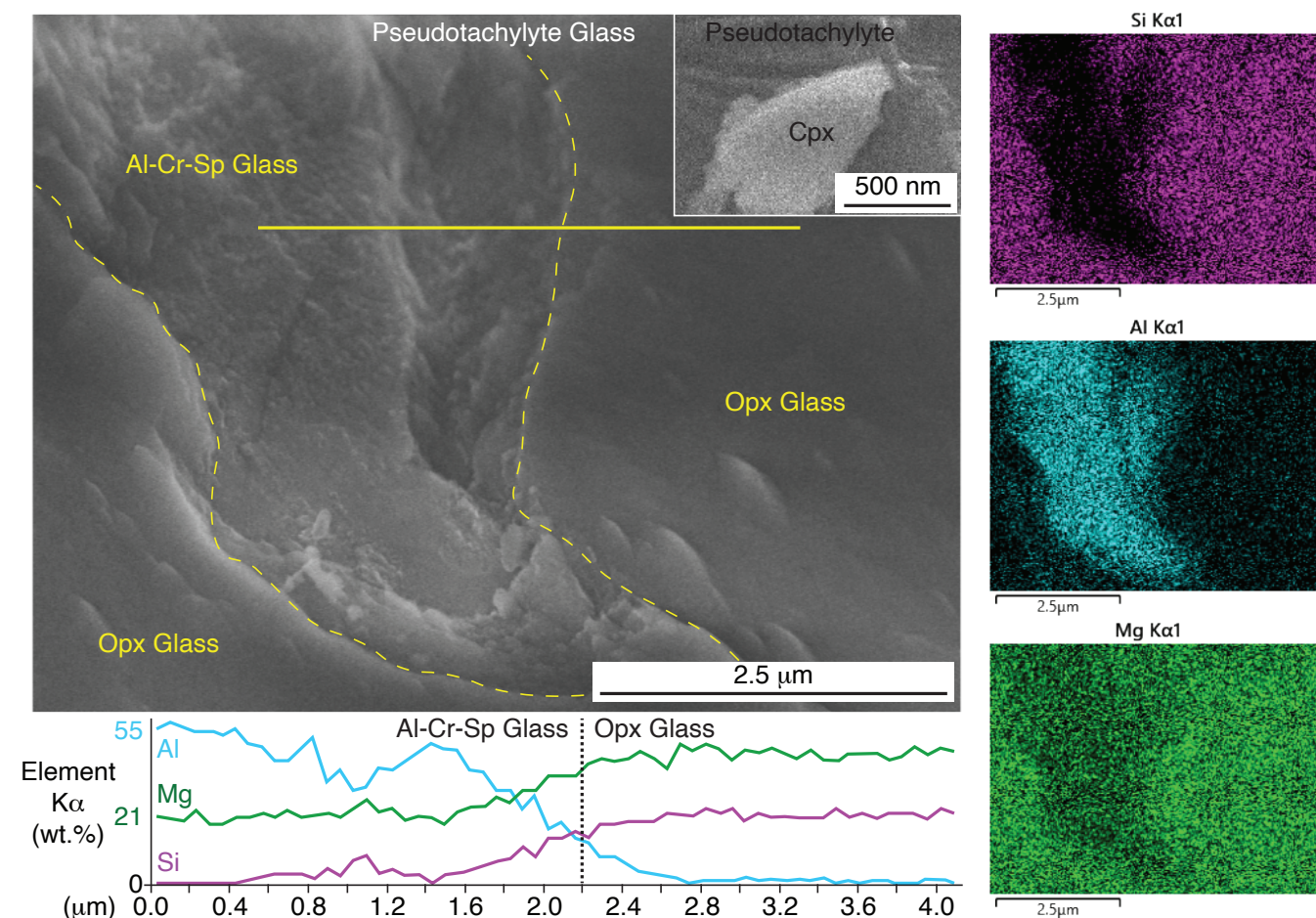


Figure 4 – Nanoscale view of pseudotachylyte. STEM-based SE image of pseudotachylyte glass and EDS analyses by applying a transect (shown as a yellow solid line) of individual analysis spots and X-ray distribution maps of Si, Al, and Mg K α from the Al-Cr spinel glassy droplet to the orthopyroxene glass droplet. The two droplets are divided by yellow dashed lines. The stippled vertical line in the chemical plot marks the point where the yellow horizontal line intersects the dashed curve in the above image. Same abbreviations as in Figure 3.

represented by clinopyroxene. Nanometer-sized clinopyroxene minerals suspended in the glass matrix may have formed by mechanical abrasion along the fault plane, yielding their angular shapes. However, they are unlikely to have experienced protracted shearing within a granular gouge as this would have resulted in rounded shapes (Ujii *et al.*, 2007). Also, crystallization of clinopyroxene in the pseudotachylyte melt upon cooling appears to be unlikely under either anhydrous conditions, which hamper fast crystallization rates, or hydrous conditions, which tend to suppress nucleation of new minerals (Mollo and Hammer, 2017). The nanoscale analysis better corroborates which fusible minerals contribute to the formation of pseudotachylytes and helps identify whether melting is congruent (a phase melts to a liquid with the same composition as the original mineral) or incongruent (a phase melts to a liquid with a composition different from the original mineral and produces a new mineral of different composition to the original mineral). Our nanoscale analysis of the glass matrix does not reveal the presence of either a melted olivine component or olivine nanocrystals. Olivine could be an expected mineral phase involved in the peritectic reaction (incongruent melting) of orthopyroxene with residual

melt with increasing temperature (Bowen, 1928). If we had applied only microscale analysis, the average bulk composition of the pseudotachylyte analyzed in the Balmuccia lherzolite (see supplementary material at Pistone, 2025) should be matched by melting 60 vol.% olivine, 27 vol.% orthopyroxene, 12 vol.% clinopyroxene, and 1 vol.% Al-Cr spinel using the set of mass balance calculations and isocon analysis described in section 3. However, the pseudotachylyte found in the Balmuccia lherzolite displays serpentinized olivine rims or devitrified pseudotachylyte glass, especially along the margins of the pseudotachylyte vein (Figure 3D), which have been unavoidably included in the EPMA analyses, as testified by the low EPMA totals (see supplementary material at Pistone, 2025). Therefore, in contrast to previous microscale analyses (Obata and Karato, 1995) and our microscale analyses of pseudotachylytes, nanoscale analysis can sufficiently distinguish the compositional heterogeneities within the glass matrix and the suspended mineral phases therein (Figure 4). In this study, nanoscale analysis helps to discriminate the components that melted alone/once (Al-Cr spinel and orthopyroxene) from unmelted components (clinopyroxene suspended in the glass; Figure 4; and olivine surrounding the pseudotachylyte;

Figure 3) and assess the “unserpentinized” composition of the pseudotachylyte. We do not find a melted olivine component anywhere in the nanoscale inspection. The absence of CaO in the pseudotachylyte composition along with the presence of clinopyroxene grains suggest the exclusion of clinopyroxene as a melted component contributing to the pseudotachylyte geochemistry. We thus propose that congruent melting of orthopyroxene and Al-Cr-spinel occurred during pseudotachylyte formation.

5.2 Are Pseudotachylytes the Result of Equilibrium or Disequilibrium Melting?

To date, pseudotachylytes have been interpreted as rocks formed under disequilibrium conditions caused by rapid cooling of melts formed rapidly during rupture and seismic slip of rocks (*Sibson, 1975; Allen, 1979; Maddock, 1986, 1992; Magloughlin, 1989; Bossière, 1991; Spray, 1992, 1993; Camacho et al., 1995; O'Hara and Sharp, 2001; Andersen and Austrheim, 2006*). However, this conventional interpretation is counterintuitive as disequilibrium cannot be explained only in terms of most effective transfer of kinematic/elastic energy to thermal energy linked to frictional heat (*Spang et al., 2024*), which then leads to frictional fusion and generation of pseudotachylyte. This efficient conversion of kinematic energy into heat is satisfied when slip velocity approaches seismic rate causing the dynamic coefficient of friction to fall to zero (*Di Toro et al., 2004*) and when heat diffusion proceeds within a timescale that is shorter or identical to the pseudotachylyte formation via melting the original rock undergoing fracturing and high-temperature friction. Thus, determining whether a phase (glass or mineral) is formed under equilibrium or disequilibrium conditions depends on the rate at which equilibrium is attained along the P - T -time path (*Powell, 1978*). In the case of formation of glassy pseudotachylyte in the Balmuccia lherzolite, frictional or flash melting is a rapid process (on the order of 0.1 to 10 seconds; *Ferrand et al. 2018*) that allows original mineral phases to melt. The formation of glassy pseudotachylytes under equilibrium conditions must include: a) the efficient diffusion of heat through the fracturing region where the pseudotachylyte forms, b) the efficient transfer of geochemical components from minerals to melt via frictional melting, c) the efficient diffusion of H_2O that helps suppress the solidus and thus, the minimum temperature required to melt the minerals forming the pseudotachylyte, d) the concomitant inefficient diffusion of chemical components that allows to identify the mineral phases fused into the pseudotachylyte melt, e) the very rapid cooling to quenching that freezes the glassy pseudotachylyte composition. Here is the detailed description of each aspect related to the generation glassy pseudotachylytes under equilibrium conditions:

a) The short timescale of frictional melting (0.1 to 10 seconds; *Ferrand et al. 2018*) forming pseudotachylytes impedes their crystallization. The efficiency of frictional melting of selective minerals without generating new

crystallites is driven by efficient thermal diffusion and large degree of undercooling that suppresses the nucleation and growth of new minerals. Thermal diffusion during pseudotachylyte formation occurs in 0.02 to 2 seconds along the pseudotachylyte-filled space of 10 μm to 1 mm (Figure 3) as thermal diffusivity in a melt is $<5 \times 10^{-7} \text{ m}^2/\text{s}$ at $>900^\circ\text{C}$ (*Romine et al., 2012*).

b) Chemical multicomponent diffusion from mineral to melt during melting becomes increasingly fast with the diffusion profile in the crystal shortening with the progress of the mineral dissolution into melt (*Zhang, 2008, 2010*).

c) Water diffuses faster than any other major element by about three orders of magnitude (*Ni and Zhang, 2008*). The in-melt diffusion of H_2O derived from hydrous minerals (amphibole; Figure 3B) and fluids commonly located along mineral grain boundaries (*Stünitz et al., 2024*) helps depress the system solidus and liquidus and impede crystallization by largely increasing the degree of undercooling (*Hort, 1998*) as H_2O diffusion takes about 100 seconds with H_2O diffusivity of $\sim 10^{-10} \text{ m}^2/\text{s}$ at limited concentrations (0.5–1 wt.%) at 1000 to 1400°C (*Van Der Laan and Wyllie, 1993; Ni and Zhang, 2008*).

d) Once the mineral phases melt at lower solidus temperature under hydrous conditions favored by efficient H_2O diffusion in the pseudotachylytic melt, the diffusion of the chemical components derived from each mineral results slow and inefficient because the diffusion of major elements such as Si, Al, and Mg having diffusivities of $3 \times 10^{-12} \text{ m}^2/\text{s}$ to $9 \times 10^{-12} \text{ m}^2/\text{s}$ in a melt (*Van Der Laan and Wyllie, 1993*) is slower than both H_2O and heat diffusion by three to five orders of magnitude (*Hofmann, 1980; Watson, 1981; Sparks and Marshall, 1986*) and, thus, slower than the rate of formation of a pseudotachylyte through melting and cooling stages.

e) Then, rapid cooling (accompanied by a large degree of undercooling that hampers crystallization) to ambient temperature on the scale of seconds to minutes following frictional melting (*O'Hara and Sharp, 2001; Andersen and Austrheim, 2006; Ferrand et al., 2018*) “freezes” the newly formed melt in the form of glass.

Therefore, the combination of efficient melting of fusible minerals and impeded crystallization during the short timescale makes the chemical composition of pseudotachylyte glass an informative snapshot of the P - T conditions of formation of pseudotachylyte under near-equilibrium conditions achieved by efficient thermal diffusion and mineral dissolution within the timescale of rock heating, melting, and solidification into glassy pseudotachylytes. This “frozen melt” records the last snapshot of P - T conditions following frictional melting envisioned as a dominant T increase under isobaric conditions as it has been proposed to date (*McKenzie and Brune, 1972; Sibson, 1975, 1980; Spray, 1992, 1995; Obata and Karato, 1995; Kanamori et al., 1998; Bouchon and Ihmlé, 1999; Hirose and Shimamoto, 2005; Di Toro et al., 2006a, 2011; Kelemen and Hirth, 2007; Lin, 2007;*

Ueda et al., 2008, 2020; Del Gaudio et al., 2009; Spang et al., 2024).

The timescale of solidification of 5-mm thick pseudotachylytes here investigated is on the order of 2 seconds, sufficient to freeze the newly formed pseudotachylyte without undergoing crystallization upon cooling. Based on the equation 3 reported in Andersen and Austrheim (2006) derived from Turcotte and Schubert (2002) detailing the solution of the Stefan problem (Stefan, 1891) applied to cooling silicate liquids, we estimate the timescale of solidification of pseudotachylyte from the Balmuccia lherzolite partial melting using these parameters: the thermal diffusivity of $5 \times 10^{-7} \text{ m}^2/\text{s}$ (Romine et al., 2012), the latent heat of melting of $5.8 \times 10^5 \text{ J/kg}$, the heat capacity of $1793 \text{ J/kg/}^\circ\text{C}$ (Leshner and Spera, 2015), and a temperature rise of 400°C (hydrous conditions) to 540°C (anhydrous conditions) as estimated using Perple_X (see sections 5.3 and 5.4) to determine the dimensionless variable of 0.81 quantifying the latent heat liberated at the solidification boundary conducted vertically upward (Turcotte and Schubert, 2002), away from the interface between partially molten pseudotachylyte and unmelted fractured rock.

We identify the two chemical components derived from the melting of mineral phases of Al-Cr spinel and orthopyroxene as two distinctive immiscible glassy droplets in the pseudotachylyte matrix (Figure 4). The slow diffusion of major elements from Al-Cr spinel and orthopyroxene allows the geochemical distinction of the two minerals as melt/glassy components through the EDS analysis (Figure 4). Furthermore, the short timescale of melting and cooling processes impedes the efficient blending or complete miscibility (Leshner and Spera, 2015) of Al-Cr spinel and orthopyroxene components. The slow chemical diffusion with respect to the short timescale of formation of pseudotachylyte hampers the generation of mineral nuclei displaying dendritic habit due to large undercooling caused by rapid cooling (i.e., quenching), heat loss or inefficient chemical diffusion through the different melt components (Fenn, 1977; Van Der Laan and Wyllie, 1993; Webber et al., 1997; Nabelek et al., 2010; Pistone et al., 2016). In addition, the large discrepancy in polymerization (i.e., viscosity) of the two melts with NBO/T of 2.36 for depolymerized orthopyroxene melt and 0.17 for polymerized Al-Cr spinel, respectively, favor their immiscibility (Jarvis et al., 2021) and distinction through geochemical analysis (Figure 4).

5.3 Petrological Assessment of Pseudotachylyte Formation Under Anhydrous Conditions

The glassy pseudotachylyte from this study is devoid of pulverized grains derived from mechanical friction, new mineral phases upon cooling, and/or cryptocrystalline phases suspended in the glass matrix at very fine spatial scale (on the order of $<2 \mu\text{m}$; Figure 4). We only identify two distinctive glasses with suspended nanometer-sized clinopyroxene crystals (Figure 4). These observations

highlight that the formation of glassy pseudotachylytes can be considered under near-equilibrium conditions based on the quantitative comparison between the timescales of heat diffusion, chemical diffusion, and solidification and the timescales of rapid melting and cooling required for pseudotachylyte formation (see section 5.2). Under such conditions we can attempt to apply thermodynamic modelling that helps reconstruct the pressure (P) and temperature (T) pathway of pseudotachylyte formation based on the collected observations at the micron (Figure 3B–D) and submicron scales including our new compositional constraints of the pristine or “unserpenititized” pseudotachylyte glassy components (Figure 4). Specifically, we can apply thermodynamic calculations to reconstruct stable mineralogy and phase diagrams for the lherzolite composition as a function of P – T conditions experienced by the Balmuccia Massif in the pre-Alpine orogenesis period from 433 to 180 Ma (Figures 5–6). We remind the reader that, during this period, A-type pseudotachylytes were generated (Souquière and Fabbri, 2010; Souquière et al., 2011; Ferré et al., 2017). These are most likely related to the peridotite exhumation during the Carboniferous Period (Ueda et al., 2008).

Below 700°C , the exhumed Balmuccia peridotite can be considered petrologically “frozen” (Ewing et al., 2015; Wyatt et al., 2022) with an average geotherm of $\sim 18^\circ\text{C/km}$ for a $\sim 40\text{-km}$ thick continental crust made of felsic granulites (using the temperature coefficient of $5 \times 10^{-4} \text{ km/s/}^\circ\text{C}$ derived from average heat flow and seismic compressional wave profiles; Blackwell 1971; Lachenbruch and Sass 1977; Christensen 1979; Christensen and Mooney 1995; Berno et al. 2020), closely related to the Paleozoic lower crust made of granulite-facies metapelites in the Ivrea-Verbano Zone (Figure 1). Herein, we evaluate the conditions of pseudotachylyte formation in P – T space using the composition of the pseudotachylyte glass (made of Al-Cr spinel and orthopyroxene) with suspended/unmelted clinopyroxene (Figures 3–4) and olivine (Figure 3). All the phases identified within and around the pseudotachylyte glass help reveal which phases effectively melted and those that did not melt during the frictional melting process. Using the anhydrous (devoid of H_2O) and hydrous (0.5–1.0 wt.% H_2O) scenarios (Figures 4–5), we aim to test two end-member processes: pure frictional melting under isobaric T increase as envisioned in previous studies (McKenzie and Brune, 1972; Sibson, 1975, 1980; Spray, 1992, 1995; Obata and Karato, 1995; Kanamori et al., 1998; Bouchon and Ihlmlé, 1999; Bjornerud and Magloughlin, 2004; Hirose and Shimamoto, 2005; Di Toro et al., 2006a, 2011; Kelemen and Hirth, 2007; Lin, 2007; Ueda et al., 2008, 2020; Del Gaudio et al., 2009; Souquière and Fabbri, 2010; Souquière et al., 2011; Kirkpatrick and Rowe, 2013; Ferrand et al., 2018; Fondriest et al., 2020; Dunkel et al., 2021; Dai et al., 2022; Moris-Muttoni et al., 2022), and fracture-induced decompression melting, newly proposed in this study.

If we consider the Balmuccia lherzolite as an anhydrous system (Figure 5), the formation of

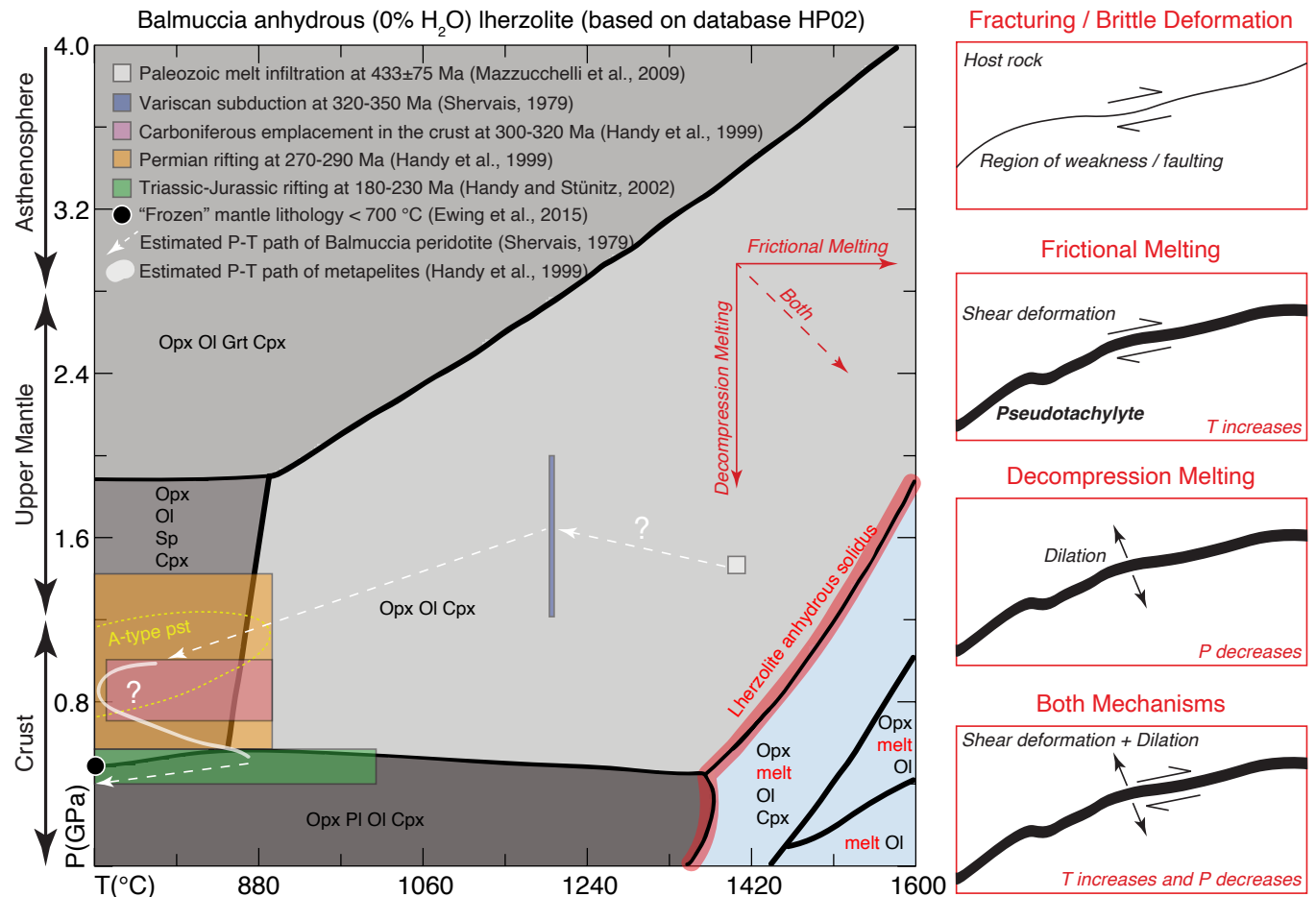


Figure 5 – P - T plot of Balmuccia anhydrous lherzolite. Perple_X-based P - T plot of Balmuccia lherzolite throughout different processes from Paleozoic to Jurassic (highlighted by dashed white arrows). Stability fields in light blue contain melt phase with the position of the anhydrous rock solidus temperature highlighted in red. The area delimited by dashed yellow line indicates the P - T conditions of A-type pseudotachylyte stability originally proposed by previous studies (Handy et al., 1999; Ueda et al., 2008). Sketches and red arrows indicate the conditions of both frictional and decompression melting in P - T space. For better display, the boundaries between different mineral assemblages are improved by manually interpolating the “step edges” of the original lines generated by the Perple_X software. Same abbreviations as in Figure 3, plus: Grt = garnet, melt = ultramafic melt, Pl = plagioclase, pst = pseudotachylyte.

pseudotachylytes during the Carboniferous Period ($T = 720$ – 900°C and $P = 0.9$ – 1.1 GPa; Handy et al. 1999; Ueda et al. 2008) requires intense friction and heat production to partially melt the minerals in the lherzolite along the fault plane. In this case, for pure frictional melting, a T increase of $\sim 540^{\circ}\text{C}$ is needed from the starting 900°C to surpass the anhydrous rock solidus temperature (Figure 5). Elastic fracture opening or shear-induced dilatancy will induce a P -drop (Samuelson et al., 2009; Nüchter, 2017; Brantut, 2019) during rock friction-induced heating (with temperature increase from the pink area of Carboniferous emplacement toward the anhydrous lherzolite solidus reported in Figure 5). This could be total (i.e., to 0 Pa), but is likely to be less because melt can migrate into the fractures and partly mitigate the pressure drop. A pressure drop does not appear to influence heat transfer (Everts and Meyer, 2018) required to induce partial melting and form pseudotachylytes. This migration of melts into open fractures becomes especially efficient and rapid when the produced melts are highly depolymerized (such as orthopyroxene liquid with $\text{NBO}/\text{T} = 2.36$) and,

thus, characterized by very low viscosity (Mysen, 1988) and in presence of high compaction length of the pore space within the fractured rock (Liang et al., 2010). For a P drop of 0.3 – 0.7 GPa, frictional melting only requires a T increase of $\sim 440^{\circ}\text{C}$ from 900°C to surpass the anhydrous rock solidus temperature (Figure 5). However, under anhydrous conditions, the melt-bearing mineral assemblage does not match the composition of the natural pseudotachylyte found in the Balmuccia lherzolite (Figure 4). Furthermore, anhydrous conditions that make the rock solidus lying at significantly high temperatures ($>1340^{\circ}\text{C}$ at 0.0001 – 0.6 GPa; Figure 5) should favor rock comminution forming fine-grained polyphase aggregates in the form of “pulverized” granular pseudotachylytes and ultramylonites (Menegon et al., 2017, 2021), whose rheology differs greatly from the generation of glassy pseudotachylytes (Figures 3-4) via partial melting considered in this study.

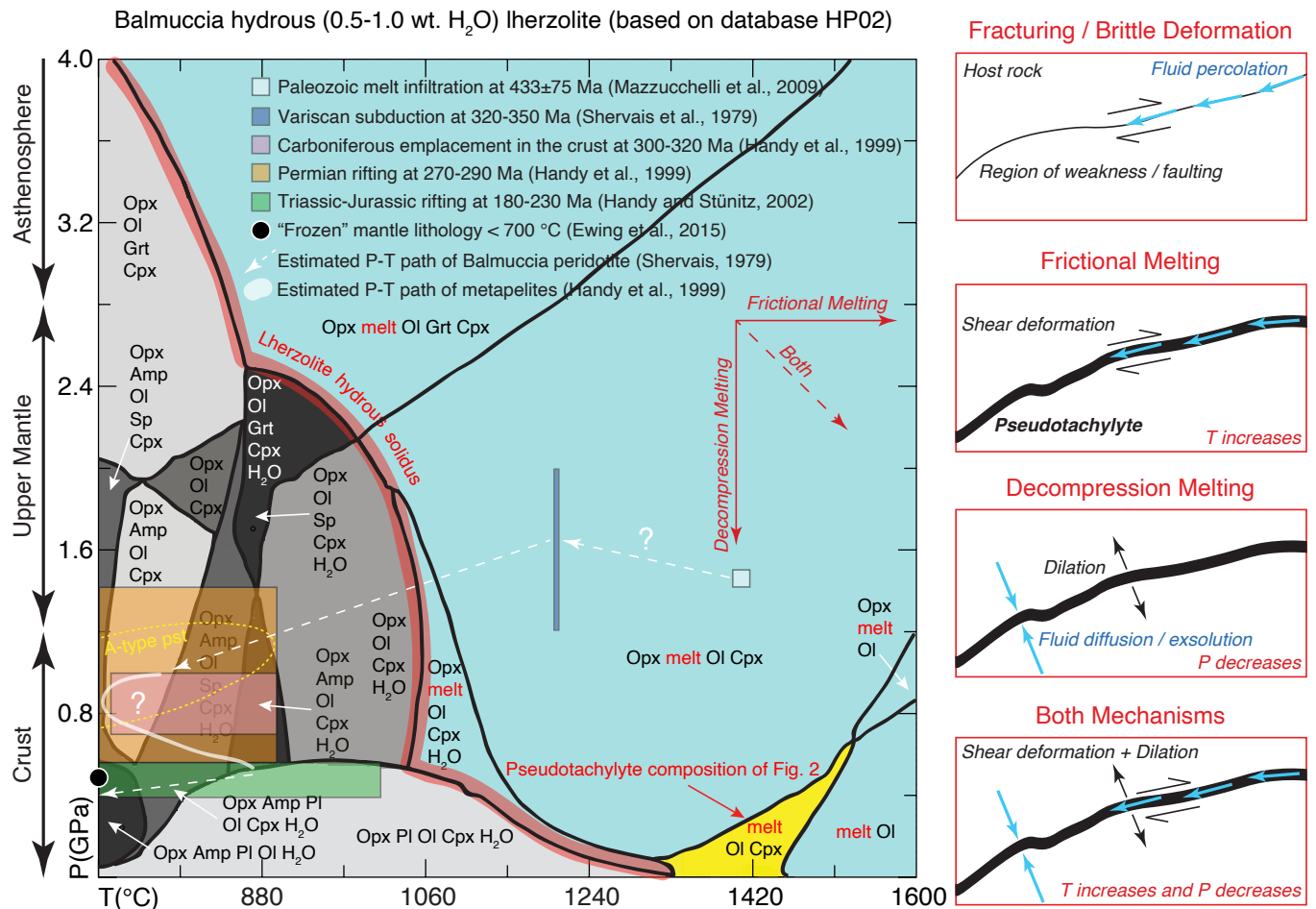


Figure 6 – P - T plot of Balmuccia hydrous (0.5-1.0 wt.% H₂O) lherzolite. Perple_X-based P - T plot of Balmuccia lherzolite throughout different processes from Paleozoic to Jurassic (highlighted by dashed white arrows). Stability fields in light blue contain melt phase with the position of the hydrous rock solidus temperature highlighted in red. The yellow field highlights that the melt composition corresponds to the pseudotachylyte composition (Al-Cr spinel- and orthopyroxene-like chemistry) with suspended clinopyroxene minerals of Figure 4 and surrounding olivine minerals of Figure 3. The area delimited by dashed yellow line indicates the P - T conditions of A-type pseudotachylyte stability originally proposed by previous studies (Handy et al., 1999; Ueda et al., 2008). Sketches and red arrows indicate the conditions of both frictional and decompression melting in P - T space in the presence of fluids (in light blue). For better display, the boundaries between different mineral assemblages are improved by manually interpolating the “step edges” of the original lines generated by the Perple_X software. Same abbreviations as in Figures 3 and 5, plus: H₂O = water as exsolved fluid.

5.4 Petrological assessment of pseudotachylyte formation under hydrous conditions and the role of decompression melting

We expect that the Balmuccia lherzolite must contain limited H₂O concentrations (0.5–1 wt.%) distributed in hydrous minerals (amphibole; Figure 3B), nominally anhydrous minerals, and/or shear zones of the mantle rock in which fluid percolation is assisted by deformation. The presence of water during the formation of pseudotachylytes is confirmed by previous studies reporting that relatively unaltered pseudotachylytes are hydrous glasses (up to 1.5 wt.% H₂O) containing vesicles, suggestive of fluid exsolution during pseudotachylyte melting at temperatures and pressures at which excess water is not soluble in the melt (Obata and Karato, 1995; O’Hara and Sharp, 2001; Ferrand et al., 2018). Presence of water in the bulk lherzolite rock expands the P - T conditions under which the rock system can

be partially molten as water helps suppresses the rock solidus to lower T conditions in a wide range of pressure (Figure 6). In this scenario, the pseudotachylyte can form by a much more limited T increase (only 160°C above 900°C) via pure frictional melting. However, to obtain a pseudotachylyte matching the chemical composition derived from melting both Al-Cr-spinel and orthopyroxene (at $T = 1300$ – 1530 °C and $P < 0.5$ GPa; Figure 6), decompression must aid frictional melting. Dilational jogs along deep crustal faults could be sites of near-total pressure release and, thus, decompression melting (Bjornerud and Magloughlin, 2004) or even boiling (forming bubbles/vesicles as documented by Obata and Karato 1995) at sufficiently low pressure (Williams, 2019). Previous work proposed that decompression melting is localized and only applies to significant depth (relevant to eclogite facies) with significant pressure drops (>1 GPa) (Bjornerud and Magloughlin, 2004). However, here we show that fracture-induced decompression melting can occur at P

<1 GPa in the granulite facies in the lower crustal section of the Ivrea-Verbano Zone (Figure 1). Indeed, a decompression of 0.3–0.9 GPa and T increase of 400°C are both required to generate Al-Cr-spinel and orthopyroxene liquids composing the ultramafic composition of the pseudotachylyte (Figure 6). This observation also supports that selective melting of minerals is more petrologically rigorous (Dobson *et al.*, 2021) than complete melting of the total rock as previous studies suggest based on microscale chemical analysis of pseudotachylytes (Obata and Karato, 1995; Ferrand *et al.*, 2018) or based on both experimental and computational simulations that illustrate how rocks experience very high temperatures due to frictional heating (Del Gaudio *et al.*, 2009; Lin and Shimamoto, 1998; Ferrand *et al.*, 2018; Woo *et al.*, 2023; Spang *et al.*, 2024). Compared to the anhydrous scenario in which T increase via frictional melting is up to ~540°C (Figure 5), water derived from hydrous minerals or external fluids facilitates both shear localization and pseudotachylyte generation (Lin and Shimamoto, 1998; O'Hara and Sharp, 2001; Andersen and Austrheim, 2006; Ferrand *et al.*, 2018). Indeed, the resulting T increase during frictional melting is reduced by 100 to 400°C corresponding to a temperature decrease of 18% to 74% (Figure 6), depending on the amount of frictional heat and pseudotachylyte melt generated in the faulted rock.

5.5 Does Overpressure Favor the Pseudotachylyte Formation?

Recently, other researchers have proposed that pseudotachylyte apophyses should be formed from overpressurized frictional melt with a pressure of 0.5 GPa greater than the lithostatic pressure (Zhong *et al.*, 2021). Melt overpressure can be caused both by volume expansion due to melting and by heating of the faulted rocks (Sibson, 1975; Swanson, 1989, 1992; Zhong *et al.*, 2021). However, this process of melt overpressurization, which is opposite to decompression, does not reproduce the geochemical composition of the pseudotachylyte inspected in this study (Figure 4). Thus, melt overpressure appears to be unfeasible within our thermodynamic constraints (Figures 5–6). Decompression melting might still be a primary process that occurs soon after fracture opening that results in pressure drop rather than pressure increase. Furthermore, such a decompression driven by fracture dilation may also be associated to dynamic stress drops related to lubrication effects of the pseudotachylyte melt as observed experimentally (Di Toro *et al.*, 2009, and references therein). Decompression melting may also prevent other effects of dilatancy, such as pressure gradients that could cause melt to flow away from where it is generated (O'Hara and Sharp, 2001; Di Toro *et al.*, 2005; Andersen and Austrheim, 2006; Ujiie *et al.*, 2007), especially if the liquids produced are highly polymerized and viscous (thereby sluggish to flow) as they derive from mineral phases enriched in network formers such as Al₂O₃ from Al-Cr spinel.

6 Conclusions

In summary, decompression associated with dilation during fracture opening in presence of water derived from hydrous minerals and fluids from grain boundaries is a crucial process facilitating the generation of pseudotachylytes in the lithosphere upon fault rupture, slip, and resultant shear heating. Water as free fluid or initially bonded in minerals suppresses the solidus of the system to lower temperature when released. Decompression melting allows pseudotachylyte to be composed of amorphous mineral phases that are consistent with relatively lower P and higher T conditions than those of the pre-failure host rock. We have demonstrated that seismic dilation can contribute to the generation of pseudotachylytes. With the analyses presented in our study, pseudotachylytes can be the consequence of a seismic rupture facilitated by water and decompression, so that less shear heating than has been proposed to date is required.

Acknowledgements

Swiss National Science Foundation (SNF) Ambizione Fellowship (PZ00P2_168166) to M.P. supported this study. Fieldwork was supported by the Terrestrial Magmatic System Research Platform of the University of Mainz (Germany). M.P. acknowledges M. Jackson (University of Utah) for the insightful discussions about her seminal works on fabrics of ultramafic rocks from the Balmuccia Peridotite Massif, for assessing the fidelity of the structural data reported in Figure 1 in this study, and for remarking the rigorous terminology applied in structural geology. The authors acknowledge the editors and all reviewers constructive inputs that helped improve our manuscript prior to publication. The authors declare that they have no competing interests. In memoriam to Luigi Burlini, scientist, mentor, and friend.

Author contributions

M.P. conceived of the idea and wrote the manuscript. M.P., V.G.T., and M.W.O. conducted fieldwork and rock sampling. M.P., M.R., and E.F. conducted the analytical investigations. All authors discussed the results and edited the manuscript.

Data availability

Data were acquired at the Georgia Electron Microscopy Center of the University of Georgia and at the electron probe micro-analyzer laboratory of the University of Lausanne. Data and supplementary material are published in a public repository: <https://doi.org/10.5281/zenodo.16884827>.

Competing interests

The authors declare no competing interests.

Peer review

This publication was peer-reviewed by Elisabetta Mariani and two anonymous reviewers. The full peer-review report can be found here: [Review Report](#).

Copyright notice

© Author(s) 2025. This article is distributed under the Creative Commons Attribution 4.0 International License, which permits unrestricted use, distribution, and reproduction in any medium, provided the original author(s) and source are credited, and any changes made are indicated.

References

- Albarede, F., and A. Provost (1977), Petrological and geochemical mass-balance equations: an algorithm for least-square fitting and general error analysis, *Computers & geosciences*, 3(2), 309–326, [https://doi.org/10.1016/0098-3004\(77\)90007-3](https://doi.org/10.1016/0098-3004(77)90007-3).
- Aldrichetti, S., G. Pennacchioni, and G. Di Toro (2025), Earthquake dynamics from pseudotachylyte microstructure, *Earth and planetary science letters*, 663(119424), 119,424, <https://doi.org/10.1016/j.epsl.2025.119424>.
- Allen, A. (1979), Mechanism of frictional fusion in fault zones, *Journal of structural geology*, 1, 231–243, [https://doi.org/10.1016/0191-8141\(79\)90042-7](https://doi.org/10.1016/0191-8141(79)90042-7).
- Andersen, T. B., and H. Austrheim (2006), Fossil earthquakes recorded by pseudotachylytes in mantle peridotite from the Alpine subduction complex of Corsica, *Earth and planetary science letters*, 242(1-2), 58–72, <https://doi.org/10.1016/j.epsl.2005.11.058>.
- Armstrong, J. T. (1988), Quantitative analysis of silicate and oxide materials: comparison of Monte Carlo ZAF and ψ (ρz) procedures, in *Microbeam analysis*, edited by D. E. Newbury, pp. 239–246, San Francisco Press Inc, San Francisco, CA.
- Austrheim, H., and T. B. Andersen (2004), Pseudotachylytes from Corsica: fossil earthquakes from a subduction complex, *Terra nova*, 16, 193–197, <https://doi.org/10.1111/j.1365-3121.2004.00551.x>.
- Baker, D. R. (1991), Interdiffusion of hydrous dacitic and rhyolitic melts and the efficacy of rhyolite contamination of dacitic enclaves, *Contributions to mineralogy and petrology. Beitrage zur Mineralogie und Petrologie*, 106(4), 462–473, <https://doi.org/10.1007/bf00321988>.
- baron de Fourier, J. B. J. (1822), *Théorie analytique de la chaleur*, Firmin Didot, Paris.
- Berno, D., R. Tribuzio, A. Zanetti, and C. Hémond (2020), Evolution of mantle melts intruding the lowermost continental crust: constraints from the Monte Capio–Alpe Cevia mafic–ultramafic sequences (Ivrea–Verbano Zone, northern Italy), *Contributions to mineralogy and petrology. Beitrage zur Mineralogie und Petrologie*, 175(1), 2, <https://doi.org/10.1007/s00410-019-1637-8>.
- Bjornerud, M., and J. F. Magloughlin (2004), Pressure-related feedback processes in the generation of pseudotachylytes, *Journal of structural geology*, 26, 2317–2323, <https://doi.org/10.1016/J.JSG.2002.08.001>.
- Blackwell, D. D. (1971), The thermal structure of the continental crust, in *The Structure and Physical Properties of the Earth's Crust, Geophysical Monograph Series*, vol. 14, edited by J. G. Heacock, pp. 169–184, AGU, Washington, D.C.
- Bossière, G. (1991), Petrology of pseudotachylytes from the alpine fault of New Zealand, *Tectonophysics*, 196, 173–193, [https://doi.org/10.1016/0040-1951\(91\)90295-4](https://doi.org/10.1016/0040-1951(91)90295-4).
- Bouchon, M., and P. Ihlmlé (1999), Stress drop and frictional heating during the 1994 Deep Bolivia Earthquake, *Geophysical research letters*, 26(23), 3521–3524, <https://doi.org/10.1029/1999gl005410>.
- Boudier, F., M. Jackson, and A. Nicolas (1984), Structural study of the Balmuccia Massif (Western Alps): A transition from mantle to lower crust, *Geologie en Mijnbouw*, 63, 179–188.
- Bowen, N. L. (1928), *The evolution of the igneous rocks*, Dover Publications, Mineola, NY.
- Bowen, N. L., and O. Andersen (1914), The binary system MgO–SiO₂, *American journal of science*, s4-37(222), 487–500, <https://doi.org/10.2475/ajs.s4-37.222.487>.
- Brack, P., P. Ulmer, and S. Schmid (2010), A crustal magmatic system from Earth mantle to the Permian surface: Field trip to the area of lower Valsesia and val d'Ossola (massiccio dei Laghi, Southern Alps, Northern Italy), *Swiss Bulletin für angewandte Geologie*, 15/2, 3–21.
- Braeck, S., Y. Y. Podladchikov, and S. Medvedev (2009), Spontaneous dissipation of elastic energy by self-localizing thermal runaway, *Physical review. E, Statistical, nonlinear, and soft matter physics*, 80(4 Pt 2), 046,105, <https://doi.org/10.1103/PhysRevE.80.046105>.
- Brantut, N. (2019), Dilatancy-induced fluid pressure drop during dynamic rupture: Direct experimental evidence and consequences for earthquake dynamics, *arXiv [physics.geo-ph]*, p. 116179, <https://doi.org/10.1016/j.epsl.2020.116179>.
- Brodie, K., and E. Rutter (1987), Deep crustal extensional faulting in the Ivrea Zone of Northern Italy, *Tectonophysics*, 140, 193–212, [https://doi.org/10.1016/0040-1951\(87\)90229-0](https://doi.org/10.1016/0040-1951(87)90229-0).
- Brodie, K., E. Rutter, and P. Evans (1992), On the structure of the Ivrea–Verbano Zone (northern Italy) and its implications for present-day lower continental crust geometry, *Terra nova*, 4, 34–40, <https://doi.org/10.1111/J.1365-3121.1992.TB00448.X>.
- Camacho, A., R. Vernon, and J. Gerald (1995), Large volumes of anhydrous pseudotachylyte in the Woodroffe Thrust, eastern Musgrave Ranges, Australia, *Journal of structural geology*, 17, 371–383, [https://doi.org/10.1016/0191-8141\(94\)00069-C](https://doi.org/10.1016/0191-8141(94)00069-C).
- Campbell, L. R., L. Menegon, A. Fagereng, and G. Pennacchioni (2020), Earthquake nucleation in the lower crust by local stress amplification, *Nature*

- communications*, 11(1), 1322, <https://doi.org/10.1038/s41467-020-15150-x>.
- Capedri, S., G. Garuti, G. Rivalenti, and A. Rossi (1977), The origin of the Ivrea-Verbano basic formation. Pyroxenitic and gabbroic mobilizates as products of the partial melting of mantle peridotite, *Neues Jahrbuch für Mineralogie, Monatshefte*, H4, 168–179.
- Christensen, N. I. (1979), Compressional wave velocities in rocks at high temperatures and pressures, critical thermal gradients, and crustal low-velocity zones, *Journal of geophysical research*, 84(B12), 6849–6857, <https://doi.org/10.1029/jb084ib12p06849>.
- Christensen, N. I., and W. D. Mooney (1995), Seismic velocity structure and composition of the continental crust: A global view, *Journal of geophysical research*, 100(B6), 9761–9788, <https://doi.org/10.1029/95JB00259>.
- Connolly, J. A. D. (1990), Multivariable phase diagrams; an algorithm based on generalized thermodynamics, *American journal of science*, 290(6), 666–718, <https://doi.org/10.2475/ajs.290.6.666>.
- Connolly, J. A. D. (2005), Computation of phase equilibria by linear programming: A tool for geodynamic modeling and its application to subduction zone decarbonation, *Earth and planetary science letters*, 236(1-2), 524–541, <https://doi.org/10.1016/j.epsl.2005.04.033>.
- Connolly, J. A. D. (2009), The geodynamic equation of state: What and how, *Geochemistry, Geophysics, Geosystems*, 10, Q10,014, <https://doi.org/10.1029/2009GC002540>.
- Connolly, J. A. D., and K. Petrini (2002), An automated strategy for calculation of phase diagram sections and retrieval of rock properties as a function of physical conditions, *Journal of metamorphic geology*, 20(7), 697–708, <https://doi.org/10.1046/j.1525-1314.2002.00398.x>.
- Creig, J. W. (1927), Immiscibility in silicate melts; Part II, *American journal of science*, 13(73), 133–154, <https://doi.org/10.2475/AJS.S5-13.74.133>.
- Dai, W., Y. Zhou, and X. Ma (2022), Pseudotachylyte-mylonites record of transient creep from inter-seismic ductile to co-seismic rupture, *Frontiers in earth science*, 10(931005), 931,005, <https://doi.org/10.3389/feart.2022.931005>.
- Dale, J., T. Holland, and R. Powell (2000), Hornblende-garnet-plagioclase thermobarometry: a natural assemblage calibration of the thermodynamics of hornblende, *Contributions to mineralogy and petrology. Beitrage zur Mineralogie und Petrologie*, 140(3), 353–362, <https://doi.org/10.1007/s004100000187>.
- Del Gaudio, P., G. Di Toro, R. Han, T. Hirose, S. Nielsen, T. Shimamoto, and A. Cavallo (2009), Frictional melting of peridotite and seismic slip, *Journal of Geophysical Research, [Solid Earth]*, 114(B6), <https://doi.org/10.1029/2008JB005990>.
- Di Toro, G., D. L. Goldsby, and T. E. Tullis (2004), Friction falls towards zero in quartz rock as slip velocity approaches seismic rates, *Nature*, 427(6973), 436–439, <https://doi.org/10.1038/nature02249>.
- Di Toro, G., G. Pennacchioni, and G. Teza (2005), Can pseudotachylytes be used to infer earthquake source parameters? An example of limitations in the study of exhumed faults, *Tectonophysics*, 402(1-4), 3–20, <https://doi.org/10.1016/j.tecto.2004.10.014>.
- Di Toro, G., T. Hirose, S. Nielsen, G. Pennacchioni, and T. Shimamoto (2006a), Natural and experimental evidence of melt lubrication of faults during earthquakes, *Science (New York, N.Y.)*, 311(5761), 647–649, <https://doi.org/10.1126/science.1121012>.
- Di Toro, G., T. Hirose, and S. Nielsen (2006b), Relating high-velocity rock-friction experiments to coseismic slip in the presence of melts, *GEOPHYSICAL*, 170, 121–134.
- Di Toro, G., G. Pennacchioni, and S. Nielsen (2009), Chapter 5 pseudotachylytes and earthquake source mechanics, in *International Geophysics, International geophysics series*, vol. 94, pp. 87–133, Elsevier, [https://doi.org/10.1016/s0074-6142\(08\)00005-3](https://doi.org/10.1016/s0074-6142(08)00005-3).
- Di Toro, G., R. Han, T. Hirose, N. De Paola, S. Nielsen, K. Mizoguchi, F. Ferri, M. Cocco, and T. Shimamoto (2011), Fault lubrication during earthquakes, *Nature*, 471(7339), 494–498, <https://doi.org/10.1038/nature09838>.
- Dobson, D. P., L. Montheil, J. J. Paine, and A. R. Thomson (2021), Peritectic melting of mica in fault-related pseudotachylyte melts and potassium mass balance as an indicator of fluid-absent source conditions, *Geochemistry, geophysics, geosystems: G(3)*, 22(2), e2020GC009217, <https://doi.org/10.1029/2020gc009217>.
- Draper, D. S., and A. D. Johnston (1992), Anhydrous PT phase relations of an Aleutian high-MgO basalt: an investigation of the role of olivine-liquid reaction in the generation of arc high-alumina basalts, *Contributions to mineralogy and petrology. Beitrage zur Mineralogie und Petrologie*, 112(4), 501–519, <https://doi.org/10.1007/bf00310781>.
- Drury, M. R., R. L. M. Vissers, D. Van der Wal, and E. H. Hoogerduijn Strating (1991), Shear localisation in upper mantle peridotites, *Pure and applied geophysics*, 137(4), 439–460, <https://doi.org/10.1007/bf00879044>.
- Dunkel, K. G., L. F. G. Morales, and B. Jamtveit (2021), Pristine microstructures in pseudotachylytes formed in dry lower crust, Lofoten, Norway, *Philosophical transactions. Series A, Mathematical, physical, and engineering sciences*, 379(2193), 20190,423, <https://doi.org/10.1098/rsta.2019.0423>.
- Ernst, W. (1981), Petrogenesis of eclogites and peridotites from the Western and Ligurian Alps, *American Mineralogist*, 66(5-6), 443–472.
- Ernst, W. G. (1978), Petrochemical study of lherzolitic rocks from the western alps, *Journal of petrology*, 19(3), 341–392, <https://doi.org/10.1093/petrology/19.3.341>.
- Everts, M., and J. P. Meyer (2018), Relationship between pressure drop and heat transfer of developing and fully developed flow in smooth horizontal circular tubes in the laminar, transitional, quasi-turbulent and turbulent flow regimes, *International journal of heat and mass transfer*, 117, 1231–1250, <https://doi.org/10.1016/j.ijheatmasstransfer.2017.10.072>.

- Ewing, T. A., D. Rubatto, M. Beltrando, and J. Hermann (2015), Constraints on the thermal evolution of the Adriatic margin during Jurassic continental break-up: U–Pb dating of rutile from the Ivrea–Verbano Zone, Italy, *Contributions to mineralogy and petrology. Beitrage zur Mineralogie und Petrologie*, 169(4), 1–22, <https://doi.org/10.1007/s00410-015-1135-6>.
- Fenn, P. M. (1977), The nucleation and growth of alkali feldspars from hydrous melts, *The Canadian mineralogist*, 15, 135–161.
- Ferrand, T. P., N. Hilaret, S. Incel, D. Deldicque, L. Labrousse, J. Gasc, J. Renner, Y. Wang, H. W. Green, Ii, and A. Schubnel (2017), Dehydration-driven stress transfer triggers intermediate-depth earthquakes, *Nature communications*, 8(1), 15,247, <https://doi.org/10.1038/ncnmms15247>.
- Ferrand, T. P., L. Labrousse, G. Eloy, O. Fabbri, N. Hilaret, and A. Schubnel (2018), Energy balance from a mantle pseudotachylyte, Balmuccia, Italy, *Journal of geophysical research. Solid earth*, 123(5), 3943–3967, <https://doi.org/10.1002/2017jb014795>.
- Ferré, E. C., A. L. Meado, and J. W. Geissman (2017), Earthquakes in the mantle? Insights from rock magnetism of pseudotachylytes, *Journal of Geophysical Research, [Solid Earth]*, 122, 8769–8785, <https://doi.org/10.1002/2017JB014618>.
- Fick, A. (1855), Ueber diffusion, *Annalen der Physik*, 170(1), 59–86, <https://doi.org/10.1002/andp.18551700105>.
- Fleet, M. E., and Y. Pan (1995), Site preference of rare earth elements in fluorapatite, *The American mineralogist*, 80(3–4), 329–335, <https://doi.org/10.2138/am-1995-3-414>.
- Fondriest, M., J. Mecklenburgh, F. X. Passelegue, G. Artioli, F. Nestola, E. Spagnuolo, M. Rempe, and G. Di Toro (2020), Pseudotachylyte alteration and the rapid fade of earthquake scars from the geological record, *Geophysical research letters*, 47(22), e2020GL090,020, <https://doi.org/10.1029/2020gl090020>.
- Garuti, G. (1977), origin Ivrea-Verbano basic formation. Microstructural data peridotites from area Sesia-Valley, *Rendiconti della Società Italiana di Mineralogia e Petrografia*, 33, 601–616.
- Garuti, G., and R. Friolo (1979), Textural features and olivine fabrics of peridotites from the Ivrea Verbano Zone, *Memorie della Società Geologica*, 33, 111–125.
- Giordano, D., and D. B. Dingwell (2003), Non-Arrhenian multicomponent melt viscosity: a model, *Earth and planetary science letters*, 208(3–4), 337–349, [https://doi.org/10.1016/s0012-821x\(03\)00042-6](https://doi.org/10.1016/s0012-821x(03)00042-6).
- Giordano, D., A. Mangiacapra, M. Potuzak, J. K. Russell, C. Romano, D. B. Dingwell, and A. Di Muro (2006), An expanded non-Arrhenian model for silicate melt viscosity: A treatment for metaluminous, peraluminous and peralkaline liquids, *Chemical geology*, 229(1–3), 42–56, <https://doi.org/10.1016/j.chemgeo.2006.01.007>.
- Giordano, D., J. K. Russell, and D. B. Dingwell (2008), Viscosity of magmatic liquids: A model, *Earth and planetary science letters*, 271(1–4), 123–134, <https://doi.org/10.1016/j.epsl.2008.03.038>.
- Grant, J. A. (1986), The isocon diagram; a simple solution to Gresens' equation for metasomatic alteration, *Economic geology*, 81, 1976–1982, <https://doi.org/10.2113/GSECONGEO.81.8.1976>.
- Grant, J. A. (2005), Isocon analysis: A brief review of the method and applications, *Physics and chemistry of the earth (2002)*, 30(17–18), 997–1004, <https://doi.org/10.1016/j.pce.2004.11.003>.
- Green, H. W., II, and H. Houston (1995), The mechanics of deep earthquakes, *Annual review of earth and planetary sciences*, 23(1), 169–213, <https://doi.org/10.1146/annurev.ea.23.050195.001125>.
- Gresens, R. L. (1967), Composition-volume relationships of metasomatism, *Chemical geology*, 2, 47–65, [https://doi.org/10.1016/0009-2541\(67\)90004-6](https://doi.org/10.1016/0009-2541(67)90004-6).
- Handy, M., and H. Stünitz (2002), Strain localization by fracturing and reaction weakening — a mechanism for initiating exhumation of subcontinental mantle beneath rifted margins, *Geological Society special publication*, 200, 387–407, <https://doi.org/10.1144/GSL.SP.2001.200.01.22>.
- Handy, M., J. Babist, R. Wagner, C. L. Rosenberg, and M. Konrad (2005), Decoupling and its relation to strain partitioning in continental lithosphere: insight from the Periadriatic fault system (European Alps), *Geological Society special publication*, 243, 249–276, <https://doi.org/10.1144/GSL.SP.2005.243.01.17>.
- Handy, M. R., L. Franz, F. Heller, B. Janott, and R. Zurbriegen (1999), Multistage accretion and exhumation of the continental crust (Ivrea crustal section, Italy and Switzerland), *Tectonics*, 18(6), 1154–1177, <https://doi.org/10.1029/1999tc900034>.
- Hartmann, G., and K. Hans Wedepohl (1993), The composition of peridotite tectonites from the Ivrea Complex, northern Italy: Residues from melt extraction, *Geochimica et cosmochimica acta*, 57(8), 1761–1782, [https://doi.org/10.1016/0016-7037\(93\)90112-a](https://doi.org/10.1016/0016-7037(93)90112-a).
- Hirose, T. (2005), Slip-weakening distance of faults during frictional melting as inferred from experimental and natural pseudotachylytes, *Bulletin of the Seismological Society of America*, 95(5), 1666–1673, <https://doi.org/10.1785/0120040131>.
- Hirose, T., and T. Shimamoto (2005), Growth of molten zone as a mechanism of slip weakening of simulated faults in gabbro during frictional melting, *Journal of geophysical research*, 110(B5), B05,202, <https://doi.org/10.1029/2004JB003207>.
- Hofmann, A. W. (1980), Diffusion in natural silicate melts: a critical review, *Physics of magmatic processes*, 385, 417.
- Holland, T., and R. Powell (1996), Thermodynamics of order-disorder in minerals; II, Symmetric formalism applied to solid solutions, *The American mineralogist*, 81(11–12), 1425–1437, <https://doi.org/10.2138/am-1996-11-1215>.
- Holland, T., and R. Powell (1998), An internally consistent thermodynamic data set for phases of petrological interest, *Journal of metamorphic geology*, 16, 309–343, <https://doi.org/10.1111/j.1525-1314.1998.00140.x>.

- Holland, T., and R. Powell (2003), Activity/composition relations for phases in petrological calculations: an asymmetric multicomponent formulation, *Contributions to mineralogy and petrology. Beitrage zur Mineralogie und Petrologie*, 145(4), 492–501, <https://doi.org/10.1007/s00410-003-0464-z>.
- Hort, M. (1998), Abrupt change in magma liquidus temperature because of volatile loss or magma mixing: Effects on nucleation, crystal growth and thermal history of the magma, *Journal of petrology*, 39(5), 1063–1076, <https://doi.org/10.1093/ptro/39.5.1063>.
- Jaeger, J. C., and N. G. W. Cook (1979), *Fundamentals of Rock Mechanics*, third ed., Chapman and Hall, London, England.
- James, T. (2001), A study of the geological structure of the Massiccio dei Laghi (Northern Italy), Ph.D. thesis, Department of Earth and Environmental Sciences, University of Manchester, United Kingdom of Great Britain and Northern Ireland.
- Jamieson, H., and P. Roeder (1984), The distribution of Mg and Fe (super 2+) between olivine and spinel at 1300 degrees C, *The American mineralogist*, 69, 283–291.
- Jarvis, P. A., M. Pistone, A. Secretan, J. D. Blundy, K. V. Cashman, H. M. Mader, and L. P. Baumgartner (2021), Crystal and volatile controls on the mixing and mingling of magmas, <https://doi.org/10.1002/9781119564485.ch6>.
- Jin, D., S.-I. Karato, and M. Obata (1998), Mechanisms of shear localization in the continental lithosphere: inference from the deformation microstructures of peridotites from the Ivrea zone, northwestern Italy, *Journal of structural geology*, 20(2-3), 195–209, [https://doi.org/10.1016/s0191-8141\(97\)00059-x](https://doi.org/10.1016/s0191-8141(97)00059-x).
- Kanamori, H., D. L. Anderson, and T. H. Heaton (1998), Frictional melting during the rupture of the 1994 bolivian earthquake, *Science (New York, N. Y.)*, 279(5352), 839–842, <https://doi.org/10.1126/science.279.5352.839>.
- Karato, S.-I., M. R. Riedel, and D. A. Yuen (2001), Rheological structure and deformation of subducted slabs in the mantle transition zone: implications for mantle circulation and deep earthquakes, *Physics of the earth and planetary interiors*, 127(1-4), 83–108, [https://doi.org/10.1016/s0031-9201\(01\)00223-0](https://doi.org/10.1016/s0031-9201(01)00223-0).
- Kelemen, P. B., and G. Hirth (2007), A periodic shear-heating mechanism for intermediate-depth earthquakes in the mantle, *Nature*, 446(7137), 787–790, <https://doi.org/10.1038/nature05717>.
- Kirkpatrick, J. D., and C. D. Rowe (2013), Disappearing ink: How pseudotachylytes are lost from the rock record, *Journal of structural geology*, 52, 183–198, <https://doi.org/10.1016/j.jsg.2013.03.003>.
- Klötzli, U., S. Sinigoi, J. E. Quick, G. Demarchi, C. Tassinari, K. Sato, and Z. Günes (2014), Duration of igneous activity in the Sesia Magmatic System and implications for high-temperature metamorphism in the Ivrea–Verbano deep crust, *Lithos*, 206, 19–33, <https://doi.org/10.1016/J.LITHOS.2014.07.020>.
- Lachenbruch, A. H., and J. H. Sass (1977), Heat flow and the thermal regime of the crust, in *The Structure and Physical Properties of the Earth's Crust, Geophysical Monograph Series*, vol. 20, edited by J. G. Heacock, pp. 626–675, AGU, Washington, D.C.
- Lensch, G. (1971), Die Ultramafite der Zone von Ivrea, *Annales Universitatis Saraviensis: Scientia*, 9, 5–146.
- Leshner, C. E., and F. J. Spera (2015), Thermodynamic and transport properties of silicate melts and magma, in *The Encyclopedia of Volcanoes*, 2 ed., pp. 113–141, Elsevier, <https://doi.org/10.1016/b978-0-12-385938-9.00005-5>.
- Liang, Y., A. Schiemenz, M. A. Hesse, E. M. Parmentier, and J. S. Hesthaven (2010), High-porosity channels for melt migration in the mantle: Top is the dunite and bottom is the harzburgite and lherzolite, *Journal of geophysical research*, 37, L15,306, <https://doi.org/10.1029/2010GL044162>.
- Lin, A. (2007), *Fossil earthquakes: The formation and preservation of pseudotachylytes, Lecture Notes in Earth Sciences*, vol. 111, 348 pp., Springer.
- Lin, A., and T. Shimamoto (1998), Selective melting processes as inferred from experimentally generated pseudotachylytes, *Journal of Asian earth sciences*, 16(5-6), 533–545, [https://doi.org/10.1016/s0743-9547\(98\)00040-3](https://doi.org/10.1016/s0743-9547(98)00040-3).
- Maddock, R. H. (1986), Partial melting of lithic porphyroclasts in fault-generated pseudotachylytes, *Neues Jahrbuch für Mineralogie – Abhandlungen*, 155, 1–14.
- Maddock, R. H. (1992), Effects of lithology, cataclasis and melting on the composition of fault-generated pseudotachylytes in Lewisian gneiss, Scotland, *Tectonophysics*, 204(3-4), 261–278, [https://doi.org/10.1016/0040-1951\(92\)90311-s](https://doi.org/10.1016/0040-1951(92)90311-s).
- Magloughlin, J. F. (1989), The nature and significance of pseudotachylyte from the Nason terrane, North Cascade Mountains, Washington, *Journal of structural geology*, 11(7), 907–917, [https://doi.org/10.1016/0191-8141\(89\)90107-7](https://doi.org/10.1016/0191-8141(89)90107-7).
- Magloughlin, J. F., and J. G. Spray (1992), Frictional melting processes and products in geological materials: introduction and discussion, *Tectonophysics*, 204(3-4), 197–204, [https://doi.org/10.1016/0040-1951\(92\)90307-r](https://doi.org/10.1016/0040-1951(92)90307-r).
- Mazzucchelli, M., G. Rivalenti, D. Brunelli, A. Zanetti, and E. Boari (2009), Formation of highly refractory dunite by focused percolation of pyroxenite-derived melt in the balmuccia peridotite massif (Italy), *Journal of petrology*, 50(7), 1205–1233, <https://doi.org/10.1093/ptrology/eg053>.
- McKenzie, D., and M. J. Bickle (1988), The volume and composition of melt generated by extension of the lithosphere, *Journal of petrology*, 29(3), 625–679, <https://doi.org/10.1093/ptrology/29.3.625>.
- McKenzie, D., and J. Brune (1972), Melting on fault planes during large earthquakes, *Geophysical journal international*, 29, 65–78, <https://doi.org/10.1111/j.1365-246X.1972.tb06152.x>.
- Menegon, L., G. Pennacchioni, N. Malaspina, K. Harris, and E. Wood (2017), Earthquakes as precursors of ductile shear zones in the dry and strong lower crust: Lower crustal

- earthquakes and mylonites, *Geochemistry, geophysics, geosystems: G(3)*, 18(12), 4356–4374, <https://doi.org/10.1002/2017gc0007189>.
- Menegon, L., L. Campbell, N. Mancktelow, A. Camacho, S. Wex, S. Papa, G. Toffol, and G. Pennacchioni (2021), The earthquake cycle in the dry lower continental crust: insights from two deeply exhumed terranes (Musgrave Ranges, Australia and Lofoten, Norway), *Philosophical transactions. Series A, Mathematical, physical, and engineering sciences*, 379(2193), 20190416, <https://doi.org/10.1098/rsta.2019.0416>.
- Menegoni, N., Y. Panara, A. Greenwood, D. Mariani, A. Zanetti, and G. Hetényi (2024), Fracture network characterisation of the Balmuccia peridotite using drone-based photogrammetry, implications for active-seismic site survey for scientific drilling, *Journal of rock mechanics and geotechnical engineering*, 16(10), 3961–3981, <https://doi.org/10.1016/j.jrmge.2024.03.012>.
- Michalchuk, S. P., S. Zertani, F. Renard, F. Fusseis, A. Chogani, O. Plümpner, and L. Menegon (2023), Dynamic evolution of porosity in lower-crustal faults during the earthquake cycle, *Journal of geophysical research. Solid earth*, 128(8), e2023JB026809, <https://doi.org/10.1029/2023jb026809>.
- Mollo, S., and J. E. Hammer (2017), Dynamic crystallization in magmas, in *Mineral reaction kinetics: Microstructures, textures, chemical and isotopic signatures*, vol. 16, pp. 378–418, Mineralogical Society of Great Britain & Ireland, <https://doi.org/10.1180/emu-notes.16.12>.
- Moris-Muttoni, B., H. Raimbourg, R. Augier, R. Champallier, and E. Le Trong (2022), The impact of melt versus mechanical wear on the formation of pseudotachylite veins in accretionary complexes, *Scientific reports*, 12(1), 1529, <https://doi.org/10.1038/s41598-022-05379-5>.
- Mysen, B. (2014), Water-melt interaction in hydrous magmatic systems at high temperature and pressure, *Progress in earth and planetary science*, 1(1), 4, <https://doi.org/10.1186/2197-4284-1-4>.
- Mysen, B. O. (1988), *Structure and properties of silicate melts*, Developments in Geochemistry, 354 pp., Elsevier Science, London, England.
- Müntener, O., P. B. Kelemen, and T. L. Grove (2001), The role of H₂O during crystallization of primitive arc magmas under uppermost mantle conditions and genesis of igneous pyroxenites: an experimental study, *Contributions to mineralogy and petrology. Beitrage zur Mineralogie und Petrologie*, 141(6), 643–658, <https://doi.org/10.1007/s004100100266>.
- Nabelek, P., A. Whittington, and M. Sirbescu (2010), The role of H₂O in rapid emplacement and crystallization of granite pegmatites: resolving the paradox of large crystals in highly undercooled melts, *Contributions to mineralogy and petrology. Beitrage zur Mineralogie und Petrologie*, 160, 313–325, <https://doi.org/10.1007/S00410-009-0479-1>.
- Ni, H., and Y. Zhang (2008), H₂O diffusion models in rhyolitic melt with new high pressure data, *Chemical geology*, 250(1-4), 68–78, <https://doi.org/10.1016/j.chemgeo.2008.02.011>.
- Nielsen, S., G. Toro, T. Hirose, and T. Shimamoto (2008), Frictional melt and seismic slip, *Journal of geophysical research*, 113, B01308, <https://doi.org/10.1029/2007JB005122>.
- Nüchter, J.-A. (2017), How vein sealing boosts fracture widening rates – The buckling-enhanced aperture growth mechanism for syn-tectonic veins, *Tectonophysics*, 694, 69–86, <https://doi.org/10.1016/j.tecto.2016.11.005>.
- Obata, M., and S.-I. Karato (1995), Ultramafic pseudotachylite from the Balmuccia peridotite, Ivrea-Verbano zone, northern Italy, *Tectonophysics*, 242(3-4), 313–328, [https://doi.org/10.1016/0040-1951\(94\)00228-2](https://doi.org/10.1016/0040-1951(94)00228-2).
- Ogawa, M. (1987), Shear instability in a viscoelastic material as the cause of deep focus earthquakes, *Journal of geophysical research*, 92(B13), 13,801–13,810, <https://doi.org/10.1029/jb092ib13p13801>.
- O'Hara, K. D., and Z. D. Sharp (2001), Chemical and oxygen isotope composition of natural and artificial pseudotachylite: role of water during frictional fusion, *Earth and planetary science letters*, 184(2), 393–406, [https://doi.org/10.1016/S0012-821X\(00\)00331-9](https://doi.org/10.1016/S0012-821X(00)00331-9).
- Pennacchioni, G., M. Scambelluri, M. Bestmann, L. Notini, P. Nimis, O. Plümpner, M. Faccenda, and F. Nestola (2024), Record of intermediate-depth subduction seismicity in a dry slab from an exhumed ophiolite, *Earth and Planetary Science Letters*, 548, 116,490.
- Peressini, G., J. E. Quick, S. Sinigoi, A. W. Hofmann, and M. Fanning (2007), Duration of a large mafic intrusion and heat transfer in the lower crust: A SHRIMP U-Pb zircon study in the ivrea-verbano zone (western alps, Italy), *Journal of petrology*, 48(6), 1185–1218, <https://doi.org/10.1093/petrology/egm014>.
- Petri, B., T. Duretz, G. Mohn, S. M. Schmalholz, G. D. Karner, and O. Müntener (2019), Thinning mechanisms of heterogeneous continental lithosphere, *Earth and planetary science letters*, 512, 147–162, <https://doi.org/10.1016/j.epsl.2019.02.007>.
- Pistone, M. (2025), Supplementary materials associated to the peer-reviewed contribution on “Can pseudotachylites form via fracture-induced decompression melting under hydrous conditions?”, published in Tektonika, <https://doi.org/10.5281/zenodo.16884827>, title of the publication associated with this dataset: Can Pseudotachylites Form via Fracture-Induced Decompression Melting Under Hydrous Conditions?
- Pistone, M., J. D. Blundy, R. A. Brooker, and EIMF (2016), Textural and chemical consequences of interaction between hydrous mafic and felsic magmas: an experimental study, *Contributions to mineralogy and petrology. Beitrage zur Mineralogie und Petrologie*, 171(1), <https://doi.org/10.1007/s00410-015-1218-4>.
- Pistone, M., L. Ziberna, G. Hetényi, M. Scarponi, A. Zanetti, and O. Müntener (2020), Joint geophysical-petrological modeling on the ivrea geophysical body beneath valsesia, Italy: Constraints on the continental lower crust, *Geochemistry, geophysics, geosystems: G(3)*, 21(12), e2020GC009397, <https://doi.org/10.1029/2020gc009397>.

- Powell, R. (1978), *Equilibrium thermodynamics in petrology*, 284 pp., Joanna Cotler Books, New York, NY.
- Quick, J. E., S. Sinigoi, and A. Mayer (1995), Emplacement of mantle peridotite in the lower continental crust, Ivrea-Verbano zone, northwest Italy, *Geology*, 23, 739–742, [https://doi.org/10.1130/0091-7613\(1995\)023<0739:EOMPIT>2.3.CO;2](https://doi.org/10.1130/0091-7613(1995)023<0739:EOMPIT>2.3.CO;2).
- Quick, J. E., S. Sinigoi, A. Snoke, T. Kalakay, A. Mayer, and G. Peressini (2002), Geologic map of the southern Ivrea-Verbano zone, northwestern Italy, *Tech. rep.*, US Geological Survey, <https://doi.org/10.3133/i2776>.
- Redler, C., T. E. Johnson, R. W. White, and B. E. Kunz (2012), Phase equilibrium constraints on a deep crustal metamorphic field gradient: metapelitic rocks from the Ivrea Zone (NW Italy): IVREA ZONE METAMORPHIC FIELD GRADIENT, *Journal of metamorphic geology*, 30(3), 235–254, <https://doi.org/10.1111/j.1525-1314.2011.00965.x>.
- Rivalenti, G., and M. Mazzucchelli (2000), Interaction of mantle derived magmas and crust in the IVZ and the Ivrea mantle peridotites, in *Crust Mantle Interactions*, edited by G. Ranalli, C. A. Ricci, and V. Trommsdorff, pp. 153–178, Siena, Italy.
- Rivalenti, G., G. Garuti, and A. Rossi (1975), The origin of the Ivrea-Verbano basic formation (western Italian Alps); whole rock geochemistry, *Bollettino della Società Geologica Italiana*, 94, 1149–1186.
- Romine, W. L., A. G. Whittington, P. I. Nabelek, and A. M. Hofmeister (2012), Thermal diffusivity of rhyolitic glasses and melts: effects of temperature, crystals and dissolved water, *Bulletin of volcanology*, 74(10), 2273–2287, <https://doi.org/10.1007/s00445-012-0661-6>.
- Rutter, E., K. Brodie, and P. Evans (1993), Structural geometry, lower crustal magmatic underplating and lithospheric stretching in the Ivrea-Verbano zone, northern Italy, *Journal of structural geology*, 15(3-5), 647–662, [https://doi.org/10.1016/0191-8141\(93\)90153-2](https://doi.org/10.1016/0191-8141(93)90153-2).
- Rutter, E., J. Khazanehdari, K. Brodie, D. Blundell, and D. Waltham (1999), Synthetic seismic reflection profile through the Ivrea zone—Serie dei Laghi continental crustal section, northwestern Italy, *Geology*, 27(1), 79–82, [https://doi.org/10.1130/0091-7613\(1999\)027<0079:SSRPTT>2.3.CO;2](https://doi.org/10.1130/0091-7613(1999)027<0079:SSRPTT>2.3.CO;2).
- Rutter, E., K. Brodie, T. James, D. J. Blundell, and D. A. Waltham (2003), Seismic modeling of lower and mid-crustal structure as exemplified by the massiccio dei Laghi (ivrea-verbano zone and serie dei Laghi) crustal section, northwestern Italy, in *Heterogeneity in the Crust and Upper Mantle*, edited by J. A. Goff and K. Holliger, pp. 67–97, Springer US, Boston, MA, https://doi.org/10.1007/978-1-4615-0103-9_3.
- Rutter, E., K. Brodie, T. James, and L. Burlini (2007), Large-scale folding in the upper part of the Ivrea-Verbano zone, NW Italy, *Journal of structural geology*, 29(1), 1–17, <https://doi.org/10.1016/j.jsg.2006.08.013>.
- Ryberg, T., C. Haberland, B. Wawerzinek, M. Stiller, K. Bauer, A. Zanetti, L. Ziberna, G. Hetényi, O. Müntener, M. Weber, and C. M. Krawczyk (2023), 3D imaging of the Balmuccia peridotite body (Ivrea-Verbano zone, NW-Italy) using controlled source seismic data, *Geophysical journal international*, 234(3), 1985–1998, <https://doi.org/10.1093/gji/ggad182>.
- Samuelson, J., D. Elsworth, and C. Marone (2009), Shear-induced dilatancy of fluid-saturated faults: Experiment and theory, *Journal of geophysical research*, 114(B12), B12,404, <https://doi.org/10.1029/2008jb0066273>.
- San Gabriel, M. L., C. Qiu, D. Yu, T. Yaguchi, and J. Y. Howe (2024), Simultaneous secondary electron microscopy in the scanning transmission electron microscope with applications for in situ studies, *Microscopy (Oxford, England)*, 73(2), 169–183, <https://doi.org/10.1093/jmicro/dfae007>.
- Scambelluri, M., G. Pennacchioni, M. Gilio, M. Bestmann, O. Plümper, and F. Nestola (2017), Fossil intermediate-depth earthquakes in subducting slabs linked to differential stress release, *Nature geoscience*, 10(12), 960–966, <https://doi.org/10.1038/s41561-017-0010-7>.
- Schaltegger, U., and P. Brack (2007), Crustal-scale magmatic systems during intracontinental strike-slip tectonics: U, Pb and Hf isotopic constraints from Permian magmatic rocks of the Southern Alps, *International journal of earth sciences*, 96(6), 1131–1151, <https://doi.org/10.1007/s00531-006-0165-8>.
- Schmid, R., and B. J. Wood (1976), Phase relationships in granulitic metapelites from the Ivrea-Verbano zone (Northern Italy), *Contributions to mineralogy and petrology. Beitrage zur Mineralogie und Petrologie*, 54(4), 255–279, <https://doi.org/10.1007/bf00389407>.
- Schmid, S. M., H. Aebli, F. Heller, and A. Zingg (1989), The role of the Periadriatic Line in the tectonic evolution of the Alps, *Geological Society special publication*, 45, 153–171, <https://doi.org/10.1144/GSL.SP.1989.045.01.08>.
- Schnetger, B. (1994), Partial melting during the evolution of the amphibolite- to granulite-facies gneisses of the Ivrea Zone, northern Italy, *Chemical geology*, 113(1-2), 71–101, [https://doi.org/10.1016/0009-2541\(94\)90006-X](https://doi.org/10.1016/0009-2541(94)90006-X).
- Shand, S. J. (1916), The pseudotachylyte of Parijs (orange free state), and its relation to ‘trap-shotten gneiss’ and ‘flinty crush-rock’, *Quarterly Journal of the Geological Society*, 72(1-4), 198–221, <https://doi.org/10.1144/gsl.jgs.1916.072.01-04.12>.
- Shervais, J. W. (1979), Thermal emplacement model for the alpine lherzolite massif at balmuccia, Italy, *Journal of petrology*, 20(4), 795–820, <https://doi.org/10.1093/petrology/20.4.795>.
- Shervais, J. W., and S. B. Mukasa (1991), The Balmuccia Orogenic Lherzolite Massif, Italy, *Journal of petrology, Special_Volume*(2), 155–174, https://doi.org/10.1093/petrology/special_volume.2.155.
- Shimamoto, T., and A. Tsutsumi (1994), A new rotary-shear high-speed frictional testing machine: Its basic design and scope of research, *Journal of Tectonic Research Group of Japan*, 39, 65–78.
- Sibson, R. (1975), Generation of pseudotachylyte by ancient seismic faulting, *Geophysical journal international*, 43,

- 775–794, <https://doi.org/10.1111/j.1365-246X.1975.tb06195.x>.
- Sibson, R. (1980), Power dissipation and stress levels on faults in the upper crust, *Journal of Geophysical Research, [Solid Earth]*, 85, 6239–6247, <https://doi.org/10.1029/JB085iB11p06239>.
- Sinigoi, S., P. Comin-Chiaramonti, G. Demarchi, and F. Siena (1983), Differentiation of partial melts in the mantle: Evidence from the Balmuccia peridotite, Italy, *Contributions to mineralogy and petrology. Beitrage zur Mineralogie und Petrologie*, 82(4), 351–359, <https://doi.org/10.1007/bf00399712>.
- Skrotzki, W., A. Wedel, K. Weber, and W. Müller (1990), Microstructure and texture in lherzolites of the Balmuccia massif and their significance regarding the thermomechanical history, *Tectonophysics*, 179, 227–251, [https://doi.org/10.1016/0040-1951\(90\)90292-G](https://doi.org/10.1016/0040-1951(90)90292-G).
- Skrotzki, W., W. Müller, and K. Weber (1991), Exsolution phenomena in pyroxenes from the Balmuccia Massif, NW-Italy, *European journal of mineralogy*, 3, 39–62, <https://doi.org/10.1127/EJM/3/1/0039>.
- Smye, A. J., L. L. Lavie, T. Zack, and D. F. Stockli (2019), Episodic heating of continental lower crust during extension: A thermal modeling investigation of the Ivrea-Verbano Zone, *Earth and planetary science letters*, 521, 158–168, <https://doi.org/10.1016/j.epsl.2019.06.015>.
- Sossi, P. A., O. Nebel, H. S. C. O'Neill, and F. Moynier (2018), Zinc isotope composition of the Earth and its behaviour during planetary accretion, *Chemical geology*, 477, 73–84, <https://doi.org/10.1016/j.chemgeo.2017.12.006>.
- Souquière, F., and O. Fabbri (2010), Pseudotachylytes in the Balmuccia peridotite (Ivrea Zone) as markers of the exhumation of the southern Alpine continental crust, *Terra nova*, 22(1), 70–77, <https://doi.org/10.1111/j.1365-3121.2009.00918.x>.
- Souquière, F., P. Monié, O. Fabbri, and A. Chauvet (2011), Polyphase seismic faulting in the Ivrea zone (Italian Alps) revealed by ⁴⁰Ar/³⁹Ar dating of pseudotachylytes: Polyphase seismic faulting in the Ivrea zone, *Terra nova*, 23(3), 162–170, <https://doi.org/10.1111/j.1365-3121.2011.00994.x>.
- Spang, A., M. Thielmann, and D. Kiss (2024), Rapid ductile strain localization due to thermal runaway, *Journal of geophysical research. Solid earth*, 129(10), e2024JB028,846, <https://doi.org/10.1029/2024jb028846>.
- Sparks, R. S. J., and L. A. Marshall (1986), Thermal and mechanical constraints on mixing between mafic and silicic magmas, *Journal of volcanology and geothermal research*, 29(1-4), 99–124, [https://doi.org/10.1016/0377-0273\(86\)90041-7](https://doi.org/10.1016/0377-0273(86)90041-7).
- Spray, J. (1993), Viscosity determinations of some frictionally generated silicate melts : Implications for fault zone rheology at high strain rates, *Journal of geophysical research*, 98, 8053–8068, <https://doi.org/10.1029/93JB00020>.
- Spray, J. (1995), Pseudotachylyte controversy: Fact or friction?, *Geology*, 23, 1119–1122, [https://doi.org/10.1130/0091-7613\(1995\)023<1119:PCFOF>2.3.CO;2](https://doi.org/10.1130/0091-7613(1995)023<1119:PCFOF>2.3.CO;2).
- Spray, J. G. (1987), Artificial generation of pseudotachylyte using friction welding apparatus: simulation of melting on a fault plane, *Journal of structural geology*, 9(1), 49–60, [https://doi.org/10.1016/0191-8141\(87\)90043-5](https://doi.org/10.1016/0191-8141(87)90043-5).
- Spray, J. G. (1992), A physical basis for the frictional melting of some rock-forming minerals, *Tectonophysics*, 204(3-4), 205–221, [https://doi.org/10.1016/0040-1951\(92\)90308-s](https://doi.org/10.1016/0040-1951(92)90308-s).
- Stefan, J. (1891), Ueber die Theorie der Eisbildung, insbesondere über die Eisbildung im Polarmeere, *Annalen der Physik*, 278(2), 269–286, <https://doi.org/10.1002/andp.18912780206>.
- Stünitz, H., H. Raimbourg, L. Nègre, J. Précigout, M. Jollands, P. Pongrac, P. Jeřábek, N. Gies, and M. Lüder (2024), Evolution of H₂O content in deforming quartz aggregates: An experimental study, *Journal of structural geology*, 178(105029), 105,029, <https://doi.org/10.1016/j.jsg.2023.105029>.
- Swanson, M. T. (1989), Sidewall ripouts in strike-slip faults, *Journal of structural geology*, 11(8), 933–948, [https://doi.org/10.1016/0191-8141\(89\)90045-x](https://doi.org/10.1016/0191-8141(89)90045-x).
- Swanson, M. T. (1992), Fault structure, wear mechanisms and rupture processes in pseudotachylyte generation, *Tectonophysics*, 204(3-4), 223–242, [https://doi.org/10.1016/0040-1951\(92\)90309-t](https://doi.org/10.1016/0040-1951(92)90309-t).
- Techmer, K. S., H. Ahrendt, and K. Weber (1992), The development of pseudotachylyte in the Ivrea–Verbano Zone of the Italian Alps, *Tectonophysics*, 204(3-4), 307–322, [https://doi.org/10.1016/0040-1951\(92\)90314-v](https://doi.org/10.1016/0040-1951(92)90314-v).
- Toffol, G., G. Pennacchioni, L. Menegon, D. Wallis, M. Faccenda, A. Camacho, and M. Bestmann (2024), On-fault earthquake energy density partitioning from shocked garnet in an exhumed seismic midcrustal fault, *Science advances*, 10(9), eadi8533, <https://doi.org/10.1126/sciadv.adi8533>.
- Trouw, R. A. J., C. W. Passchier, and D. J. Wiersma (2010), *Atlas of Mylonites - and related microstructures*, 26–43 pp., Springer, Berlin, Germany, <https://doi.org/10.1007/978-3-642-03608-8>.
- Tsutsumi, A., and T. Shimamoto (1997a), High-velocity frictional properties of gabbro, *Geophysical research letters*, 24(6), 699–702, <https://doi.org/10.1029/97gl00503>.
- Tsutsumi, A., and T. Shimamoto (1997b), Temperature measurements along simulated faults during seismic fault motion, in *Proceedings of the 30th International Geological Congress*, vol. 5, pp. 223–232.
- Turcotte, D. L., and G. Schubert (2002), *Geodynamics*, 472 pp., Cambridge university press, Cambridge, England.
- Ueda, T., M. Obata, G. Di Toro, K. Kanagawa, and K. Ozawa (2008), Mantle earthquakes frozen in mylonitized ultramafic pseudotachylytes of spinel-lherzolite facies, *Geology*, 36(8), 607, <https://doi.org/10.1130/g24739a.1>.
- Ueda, T., M. Obata, K. Ozawa, and I. Shimizu (2020), The ductile-to-brittle transition recorded in the balmuccia peridotite body, Italy: Ambient temperature for the onset of seismic rupture in mantle rocks, *Journal of geophysical*

- research. *Solid earth*, 125(2), e2019JB017385, <https://doi.org/10.1029/2019jb017385>.
- Ujiie, K., H. Yamaguchi, A. Sakaguchi, and S. Toh (2007), Pseudotachylites in an ancient accretionary complex and implications for melt lubrication during subduction zone earthquakes, *Journal of structural geology*, 29(4), 599–613, <https://doi.org/10.1016/j.jsg.2006.10.012>.
- Van Der Laan, S. R., and P. J. Wyllie (1993), Experimental interaction of granitic and basaltic magmas and implications for mafic enclaves, *Journal of petrology*, 34(3), 491–517, <https://doi.org/10.1093/petrology/34.3.491>.
- Voshage, H., A. W. Hofmann, M. Mazzucchelli, G. Rivalenti, S. Sinigoi, I. Raczek, and G. Demarchi (1990), Isotopic evidence from the Ivrea Zone for a hybrid lower crust formed by magmatic underplating, *Nature*, 347(6295), 731–736, <https://doi.org/10.1038/347731a0>.
- Watson, E. B. (1981), Diffusion in magmas at depth in the Earth: The effects of pressure and dissolved H₂O, *Earth and planetary science letters*, 52(2), 291–301, [https://doi.org/10.1016/0012-821x\(81\)90184-9](https://doi.org/10.1016/0012-821x(81)90184-9).
- Watson, E. B. (1982), Basalt contamination by continental crust: Some experiments and models, *Contributions to mineralogy and petrology. Beitrage zur Mineralogie und Petrologie*, 80(1), 73–87, <https://doi.org/10.1007/bf00376736>.
- Webber, K. L., A. U. Falster, W. B. Simmons, and E. E. Foord (1997), The role of diffusion-controlled oscillatory nucleation in the formation of line rock in pegmatite-plite dikes, *Journal of petrology*, 38(12), 1777–1791, <https://doi.org/10.1093/ptro/38.12.1777>.
- Wenk, H. (1978), Are pseudotachylites products of fracture or fusion, *Geology*, 6(8), 507–511, [https://doi.org/10.1130/0091-7613\(1978\)6<507:APPOFO>2.0.CO;2](https://doi.org/10.1130/0091-7613(1978)6<507:APPOFO>2.0.CO;2).
- Wiederkehr, M., R. Bousquet, S. Schmid, and A. Berger (2008), From subduction to collision: Thermal overprint of HP/LT meta-sediments in the north-eastern Lepontine Dome (Swiss Alps) and consequences regarding the tectono-metamorphic evolution of the Alpine orogenic wedge, *Swiss Journal of Geosciences*, 101, 127–155, <https://doi.org/10.1007/s00015-008-1289-6>.
- Wiederkehr, M., M. Sudo, R. Bousquet, A. Berger, and S. M. Schmid (2009), Alpine orogenic evolution from subduction to collisional thermal overprint: The 40Ar/39Ar age constraints from the Valaisan Ocean, central Alps: DATING IN POLYMETAMORPHIC METASEDIMENTS, *Tectonics*, 28(6), TC6009, <https://doi.org/10.1029/2009tc002496>.
- Williams, R. T. (2019), Coseismic boiling cannot seal faults: Implications for the seismic cycle, *Geology*, 47(5), 461–464, <https://doi.org/10.1130/g45936.1>.
- Woo, S., R. Han, and K. Ohashi (2023), Frictional melting mechanisms of rocks during earthquake fault slip, *Scientific reports*, 13(1), 12,563, <https://doi.org/10.1038/s41598-023-39752-9>.
- Wyatt, D. C., A. J. Smye, J. M. Garber, and B. R. Hacker (2022), Assembly and tectonic evolution of continental lower crust: Monazite petrochronology of the ivrea-verbano zone (val strona di omegna), *Tectonics*, 41(3), e2021TC006841, <https://doi.org/10.1029/2021tc006841>.
- Yao, L., S. Ma, and G. Di Toro (2023), Coseismic fault sealing and fluid pressurization during earthquakes, *Nature communications*, 14(1), 1136, <https://doi.org/10.1038/s41467-023-36839-9>.
- Zhan, Z. (2020), Mechanisms and implications of deep earthquakes, *Annual review of earth and planetary sciences*, 48(1), 147–174, <https://doi.org/10.1146/annurev-earth-053018-060314>.
- Zhang, Y. (2008), *Geochemical Kinetics*, Princeton University Press, Princeton, NJ.
- Zhang, Y. (2010), Diffusion in minerals and melts: Theoretical background, *Reviews in mineralogy and geochemistry*, 72(1), 5–59, <https://doi.org/10.2138/rmg.2010.72.2>.
- Zhong, X., A. J. Petley-Ragan, S. H. M. Incel, M. Dabrowski, N. H. Andersen, and B. Jamtveit (2021), Lower crustal earthquake associated with highly pressurized frictional melts, *Nature geoscience*, 14(7), 519–525, <https://doi.org/10.1038/s41561-021-00760-x>.
- Zingg, A. (1983), The Ivrea and Strona-Ceneri zones (Southern Alps, Ticino and N-Italy) - a review, *Schweizerische mineralogische und petrographische Mitteilungen*, 63, 361–392.
- Zingg, A., and J. C. Hunziker (1990), The age of movements along the Insubric Line west of Locarno (northern Italy and southern Switzerland), *Eclogae Geologicae Helvetiae*, 83, 629–644.